

This discussion paper is/has been under review for the journal *Atmospheric Chemistry and Physics (ACP)*. Please refer to the corresponding final paper in *ACP* if available.

**Assessment of  
vertically-resolved  
PM<sub>10</sub>**

J.-C. Raut and  
P. Chazette

# Assessment of vertically-resolved PM<sub>10</sub> from mobile lidar observations

J.-C. Raut<sup>1</sup> and P. Chazette<sup>2</sup>

<sup>1</sup>Laboratoire de Météorologie Dynamique, Ecole Polytechnique, 91128 Palaiseau, France

<sup>2</sup>Laboratoire des Sciences du Climat et de l'Environnement, Laboratoire mixte  
CEA-CNRS-UVSQ, CEA Saclay, 91191 Gif-sur-Yvette, France

Received: 28 April 2009 – Accepted: 4 June 2009 – Published: 18 June 2009

Correspondence to: J.-C. Raut (jean-christophe.raut@lmd.polytechnique.fr)

Published by Copernicus Publications on behalf of the European Geosciences Union.

Title Page

Abstract

Introduction

Conclusions

References

Tables

Figures

⏪

⏩

◀

▶

Back

Close

Full Screen / Esc

Printer-friendly Version

Interactive Discussion

## Abstract

We investigate in this study the role of the Paris Peripherique (the ring around Paris agglomeration) in local particulate pollution and the horizontal gradient of pollution between Paris centre and its remote suburbs. For this purpose, we combine in situ surface measurements with active remote sensing observations obtained from a great number of research programs in Paris area since 1999. Two approaches, devoted to the conversion of vertical profiles of lidar-derived extinction coefficients into  $PM_{10}$ , have been set up. A very good agreement is found between the theoretical and empirical methods with a discrepancy of 3%. Hence, specific extinction cross-sections at 355 nm are provided with a reasonable uncertainty for urban ( $4.5 \text{ m}^2/\text{g}$ ), periurban ( $5.9 \text{ m}^2/\text{g}$ ), rural ( $7.1 \text{ m}^2/\text{g}$ ), biomass burning ( $2.6 \text{ m}^2/\text{g}$ ) and dust ( $1.1 \text{ m}^2/\text{g}$ ) aerosols. The high spatial and temporal resolutions of the mobile lidar (respectively 1.5 m and 1 min) enable to follow the spatiotemporal variability of various layers carrying aerosols in the troposphere. Appropriate specific extinction cross-sections are applied in each layer detected in the vertical heterogeneities from the lidar profiles. The standard deviation between lidar-derived  $PM_{10}$  at 200 m above ground and surface network stations measurements was  $\sim 14 \mu\text{g m}^{-3}$ . This difference is particularly ascribed to a decorrelation of mass concentrations in the first meters of the boundary layer, as highlighted through multiangular lidar observations. Lidar signals can be used to follow mass concentrations at the surface and provide useful information on  $PM_{10}$  peak forecasting that affect air quality.

## 1 Introduction

Aerosol studies experience a revival of interest since human activities tend to increase their concentrations in the atmosphere. The anthropogenic aerosols currently account for about 10 percent of the total mass concentration of aerosols over the globe. During the last decades, epidemiological studies have identified a link between pollution

### Assessment of vertically-resolved $PM_{10}$

J.-C. Raut and  
P. Chazette

Title Page

Abstract

Introduction

Conclusions

References

Tables

Figures

⏪

⏩

◀

▶

Back

Close

Full Screen / Esc

Printer-friendly Version

Interactive Discussion

by airborne particulate matter (PM) and health hazards such as respiratory (allergies, asthma, altered lung function) and cardiovascular diseases (Dockery et al., 1993). Particle toxicity depends on its concentration and chemical composition, but also and foremost of its size since the smallest aerosols are recognized to be the most harmful given that they can reach human breathing apparatus down to the pulmonary cells (Donaldson et al., 1998). At urban scale, issues addressing atmospheric pollution concern pollution peaks forecasting and their corresponding factors, both influencing the air quality and its impact on public health. This becomes an important research area in megacities, which are in full expansion and whose number is going to increase during the 21st century. In such large urban centers, local experimental studies have already been devoted to the microphysical, chemical and optical characterization of urban aerosols: Athens (Kambeizidis et al., 1995), Los Angeles (e.g. Lurmann et al., 1997), Sao Paulo (e.g. Landulfo et al., 2003), Marseilles (e.g. Mestayer et al., 2005) or Paris (e.g. Randriamiarisoa et al., 2006). In such an industrialised region, the main source of photo-oxidant pollution turns out to be automobile traffic auto (e.g. Menut et al., 2000; Chazette et al., 2005b). Air quality over Paris is continuously surveyed by a dedicated surface network carrying out measurements of critical pollutant concentrations, aerosols in particular (AIRPARIF, <http://www.airparif.asso.fr/>).

However, surface measurements are not sufficient to fully understand the pollutants dynamics and chemistry. Forecasting pollution peaks are mainly constrained using ground-based observations (e.g. Hodzic et al., 2006; Tombette et al., 2008). The improvement of PM prediction, required for driving emission reduction strategies, needs a thorough understanding of the processes affecting aerosol concentrations as well as vertically-resolved measurements in the atmospheric column. This can now be achieved thanks to the new generation of portable lidar systems developed in the past five years (e.g. Raut and Chazette, 2007; Chazette and al., 2007). Such active remote sensing instruments document the mid and lower troposphere by means of aerosol optical properties. Yet, health standards defined in Europe and especially in France (European directive no. 1999/30/CE of 22 April 1999) for particulate pollution impose

---

**Assessment of  
vertically-resolved  
PM<sub>10</sub>**J.-C. Raut and  
P. Chazette

---

Title Page

Abstract

Introduction

Conclusions

References

Tables

Figures

⏪

⏩

◀

▶

Back

Close

Full Screen / Esc

Printer-friendly Version

Interactive Discussion

a monitoring from surface measurements of aerosol mass concentrations in terms of aerodynamic diameter lower than  $10\ \mu\text{m}$  ( $\text{PM}_{10}$ ). Such a boundary has been reduced to  $2.5\ \mu\text{m}$  ( $\text{PM}_{2.5}$ ) in United-States (e.g. Parkhurst et al., 1999). As an alternative to gravimetric measurements, one direction is to use the optical properties of the aerosols to estimate their abundance. As a consequence, the challenge is to convert vertically-resolved optical measurements into mass concentrations and this requires instruments with a fine vertical resolution.

We focus in this study on the retrieval of  $\text{PM}_{10}$  from ground-based and mobile lidar systems over the Paris megalopolis area ( $\sim 12$  millions inhabitants). The choice of this agglomeration has been driven by the need of a sufficiently representative database to establish a reliable relation between mass concentration and optical properties of pollution aerosol. It is the case in Paris area, where a great number of research programs has been carried out since 1998 with the ESQUIF project (Vautard et al., 2003). Hence, this study lies on observations performed during ESQUIF in 1999 (Chazette et al., 2005b; Raut and Chazette, 2008a), MEAUVE (Modélisation des Effets des Aérosols en Ultra Violet et Expérimentation) in 2001 (Lavigne et al., 2005), LISAIR (Lidar pour la Surveillance de l’AIR) in 2005 (Raut and Chazette, 2007) and ParisFog in 2007 (Elias et al., 2009; Haeffelin et al., 2009) campaigns.

This paper investigates for the first time the role of the Paris Peripherique (the ring around Paris agglomeration) in local particulate pollution and the horizontal gradient of pollution between Paris centre and its remote suburbs. Section 2 presents the lidar systems involved in the experiment, as well as in situ instrumentation. Section 3 describes the methodology to derive mass from aerosol optical parameters. The corresponding results obtained during the different campaigns are presented in Sect. 4. Observations of the different aerosol layers converted in  $\text{PM}_{10}$  are described in Sect. 5. In the Sect. 6 we discuss the relations between the surface mass concentration measurements performed by the operational air quality network and the lidar-derived mass concentration profiles. We conclude in a seventh section.

---

**Assessment of  
vertically-resolved  
 $\text{PM}_{10}$** J.-C. Raut and  
P. Chazette

---

Title Page

Abstract

Introduction

Conclusions

References

Tables

Figures

⏪

⏩

◀

▶

Back

Close

Full Screen / Esc

Printer-friendly Version

Interactive Discussion

## 2 Experimental set-up

### 2.1 Location sites

Specific experiments involving both lidar systems and ground-based in situ instruments were performed in Paris area (UTC+2 h) from 1999 to 2007. In this study, we consider four experimental sites corresponding to urban, periurban and rural locations. Two experiments were performed in Paris (48°51'24" N, 2°21'07" E): the ESQUIF campaign in July 1999 (Chazette et al., 2005b; Randriamiarisoa et al., 2006) and the LISAIR (Raut and Chazette, 2007) experiment in May 2005. The periurban sites are located at ~15 km in the South-West of Paris: Saclay (48°43'51" N, 2°10'21" E) in the framework of the ESQUIF project in July 1999 (Randriamiarisoa et al., 2006) and Palaiseau (48°42'52" N, 2°14'45" E) (Elias et al., 2009; Haeffelin et al., 2009) during the 6-months long Parisfog campaign carried out from October 2006 to March 2007. The rural site is Brétigny (48°36'41" N, 2°18'21" E), ~30 km far from Paris, where MEAUVE experiment was conducted in March 2001 (Lavigne et al., 2005).

### 2.2 Instruments

The *Lidar Aérosol UltraViolet (LAUV-EZ lidar®)* system is a homemade prototype backscatter lidar emitting in the ultraviolet developed by the Commissariat à l'Energie Atomique (CEA) and the Centre National de la Recherche Scientifique (CNRS) (Chazette et al., 2007). It is now commercialized by the LEOSPHERE Company under the name of EZ Lidar® (www.leosphere.com). It is designed to monitor the aerosol dispersion in the low and middle troposphere. It operates with a Nd:Yag laser at the wavelength of 355 nm. It is light, compact, eye-safe and suitable for a mobile platform. The resolution along the line of sight is 1.5 m. For this experiment, it was operated onboard small personal vehicle. The advantage of such a small car is its excellent manoeuvrability in small atmospheric volumes. The lidar measurement is associated with an overlap factor close to 1 at ~100 m above the ground level (a.g.l.).

## Assessment of vertically-resolved PM<sub>10</sub>

J.-C. Raut and  
P. Chazette

Title Page

Abstract

Introduction

Conclusions

References

Tables

Figures

⏪

⏩

◀

▶

Back

Close

Full Screen / Esc

Printer-friendly Version

Interactive Discussion

---

**Assessment of  
vertically-resolved  
PM<sub>10</sub>**J.-C. Raut and  
P. Chazette

---

Title Page

Abstract

Introduction

Conclusions

References

Tables

Figures

⏪

⏩

◀

▶

Back

Close

Full Screen / Esc

Printer-friendly Version

Interactive Discussion

The *Lidar pour l'Etude et le Suivi de l'Aérosol Atmosphérique (LESAA)* was developed by the Commissariat à l'Energie Atomique (CEA) to measure the atmospheric reflectivity at 355 or 532 nm in the lower troposphere over polluted areas. It is a part of the instrumental payload of the Mobile Aerosol Station (SAM, Chazette et al., 2005a).

LESAA uses aerosol backscattering to examine the lower troposphere structure with a vertical resolution of 7.5 m (Chazette et al., 2005a). The sky background radiance is measured from the lidar signal at high altitude (45 to 55 km) where the laser beam is considered to be negligible. The lidar measurement is associated with an overlap factor close to 1 at ~200 m above the ground level (a.g.l.).

A *three-wavelength (450, 550 and 700 nm) nephelometer* (manufactured by TSI) Model 3563 was used onboard SAM to measure the aerosol scattering coefficient of particles with a diameter larger than 0.05 μm in a 7–170° range of scattering angle (Bodhaine et al., 1991) every minute at a flow rate of 20 L/min. The three wavelength instrument scattering chamber was maintained at about 35–40% relative humidity. To take into account the non-observed scattering angles, a correction factor has been assessed, from Mie computations, to be close to 1.03 for urban aerosols. Relative uncertainty on the measurements is close to 5%.

The particle measurements were performed using automatic *TEOM (Tapered Element Oscillating Microbalance, Rupprecht and Pataschnik)* Model 1400 A instruments equipped with a PM<sub>10</sub> inlet at a flow rate of 1 m<sup>3</sup>/h. The air is heated inside the instruments to 50°C in order to remove any water on the particles. Mass concentrations are obtained every minute with a maximum absolute uncertainty of 5 μg m<sup>-3</sup>. One TEOM instrument is included in the operational air quality network AIRPARIF and another one is part of the SAM payload.

The *Electrical Low Pressure Impactor (ELPI)* is a real-time particle size spectrometer designed at the Tampere University of Technology (Delkati, Ltd., <http://dekati.com/cms/elpi>) for real-time monitoring of aerosol particle size distribution (Keskinen et al., 1992). It has been recently included in the instrumental payload of SAM. The ELPI measures airborne particle size distribution from 0.028 to 10.03 μm within 12 channels every

minute with a flow rate of 10 L/min. The accuracy on the aerosol number concentration measurement is about 5%.

Aerosol samples devoted to carbonaceous analyses were collected on pre-cleaned *Whatman GF/F glass-fiber filters*. The carbon mass was determined through a thermal protocol (Cachier et al., 1989). The precision of the results is estimated to be of the order of 10%. *Whatman nuclepore membranes* in polycarbonate were also mounted on stack filters unit. Those filters were used for measuring the major water soluble (WS) inorganic cations ( $\text{Na}^+$ ,  $\text{NH}_4^+$ ,  $\text{K}^+$ ,  $\text{Mg}^{2+}$ ,  $\text{Ca}^{2+}$ ) and anions ( $\text{Cl}^-$ ,  $\text{NO}_3^-$ ,  $\text{SO}_4^{2-}$ ) in the particle by ion chromatography (DIONEX DX600). The sensitivity of ionic analyses is  $\sim 0.1$  ppb and blank concentrations are lower than 30 ppb for each species. The precision on ion chromatography analysis has been evaluated to be 5–10% (Chazette and Liousse, 2001).

A *Vaisala meteorological probe* type PTU200 onboard SAM was used to measure the temperature (with an uncertainty of  $\sim 0.1$  K), the relative humidity ( $\sim 1\%$ ), and the atmospheric pressure ( $\sim 1$  hPa).

To study the influence of air masses motion in the low troposphere, a two-dimensional *SONIC anemometer* was used at the location of in situ instrumentation. It provides real-time and continuous measurements of air velocity in horizontal directions and also temperature.

## 3 Methodology to convert aerosol extinction coefficient into $\text{PM}_{10}$

### 3.1 General context

Studies devoted to relationships between PM concentrations and optical thicknesses retrieved from passive remote sensing instruments have received considerable attention and have underlined a good potential for aerosol optical properties to be used in air quality studies (Shinozuka et al., 2007). Chu et al. (2003) showed a fairly reasonable correlation between daily averaged values of  $\text{PM}_{10}$  and aerosol optical thicknesses

## Assessment of vertically-resolved $\text{PM}_{10}$

J.-C. Raut and  
P. Chazette

Title Page

Abstract

Introduction

Conclusions

References

Tables

Figures

⏪

⏩

◀

▶

Back

Close

Full Screen / Esc

Printer-friendly Version

Interactive Discussion

**Assessment of  
vertically-resolved  
PM<sub>10</sub>**J.-C. Raut and  
P. Chazette

Title Page

Abstract

Introduction

Conclusions

References

Tables

Figures

◀

▶

◀

▶

Back

Close

Full Screen / Esc

Printer-friendly Version

Interactive Discussion

(AOT) at 550 nm derived from AERONET (Aerosol Robotic Network; Holben et al., 1998). Similarly in Alabama, Wang and Christopher (2003) linearly correlated mean hourly PM<sub>2.5</sub> measurements from a TEOM and satellite MODIS (Moderate Resolution Imaging Spectroradiometer) derived AOT at 550 nm. Liu et al. (2004) proposed annual mean ground-level PM<sub>2.5</sub> concentration maps using the Multiangle Imaging Spectroradiometer (MISR) AOT over the continuous United States.

Those studies were however limited by the total aerosol loading over the whole atmospheric column. Pelletier et al. (2007) found that a linear model failed at explaining the data well but that the performance could be significantly improved when such a linear relationship would be conditioned on auxiliary parameters, mainly meteorological variables. The knowledge of vertical profiles of PM concentrations would be also an important step for public health related studies. Van Dokelaar et al. (2006) suggested that the relative vertical profile of aerosol extinction is the dominant parameter in determining the spatial variation between AOT and PM<sub>2.5</sub> over North America. In this section, we try to establish the link between aerosol extinction coefficient and PM<sub>10</sub> concentration measured at surface. Such relationships will be then extended to vertical profiles of extinction coefficients as retrieved from lidar measurements.

### 3.2 Empirical linear relationship between PM<sub>10</sub> and aerosol extinction coefficient

Linear relationships between PM<sub>10</sub> and aerosol extinction coefficient at 355 nm ( $\alpha_{\text{ext},355}$ ) have been fully investigated in Raut et al. (2009). They can be written under the form:

$$\text{PM}_{10} = k_1 \cdot \alpha_{\text{ext},355} \quad (1)$$

At the surface, the extinction coefficient is not measured directly. It is derived from the aerosols scattering coefficient at 700 nm  $\alpha_{\text{scat},700}$ , the scattering Angström exponent between 450 and 700 nm  $\alpha$ , both retrieved from the nephelometer, and the single-



scattering albedo at 355 nm  $\omega_{0,355}$ :

$$PM_{10} = \frac{k_1}{\omega_{0,355}} \cdot \left(\frac{355}{700}\right)^{-a} \cdot \alpha_{\text{scat},700} \quad (2)$$

$\omega_{0,355}$  is determined from Mie calculations performed with the number size distribution and the complex refractive index. This latter can be obtained through a simple volume-linear internal mixing rule from the refractive indices of the aerosol chemical compounds measured on the filters. An alternative approach to retrieve the complex refractive index, developed by Raut and Chazette (2007, 2008a), lies on a closure study between active and remote sensing observations as well as in situ measurements. The corresponding uncertainty  $\sigma_{k_1}$  on  $k_1$  is given by the respective uncertainties  $\sigma_{\omega_0}$ ,  $\sigma_a$ , and  $\sigma_{C_0}$  on  $\omega_{0,355}$ ,  $a$  and  $C_0$ , the slope of the regression analysis between  $\alpha_{\text{scat},700}$  and  $PM_{10}$ :

$$\frac{\sigma_{k_1}}{k_1} = \left[ \left(\frac{\sigma_{\omega_0}}{\omega_0}\right)^2 + \left(\frac{\sigma_{C_0}}{C_0}\right)^2 + \left(\sigma_a \cdot \ln\left(\frac{355}{700}\right)\right)^2 \right]^{1/2} \quad (3)$$

### 3.3 Theoretical relationship between $PM_{10}$ and extinction coefficient

Aerosol extinction coefficient and  $PM_{10}$  are related at the instant ( $i$ ) by

$$PM_{10}^{(i)} = \rho \cdot \frac{4}{3} \pi \cdot \frac{\overline{r^3}^{(i)}}{\overline{\sigma_{\text{ext},355}}^{(i)}} \cdot \alpha_{\text{ext},355}^{(i)} \quad (4)$$

Where  $\overline{r^3}^{(i)}$  is the mean cubic radius, calculated from the size distribution and  $\overline{\sigma_{\text{ext},355}}^{(i)}$  is the mean extinction cross-section at 355 nm over the size range considered at the instant  $i$ , and  $\rho$  is the density of particles. In this paper, the density is estimated using the mass of ions, organic compounds and black carbon reported on the chemical filters analyses. The theoretical relationship has been established by Raut et al. (2009) as:

$$PM_{10}^{(i)} = k_2 \cdot \alpha_{\text{ext},355}^{(i)} \quad (5)$$

Assessment of  
vertically-resolved  
 $PM_{10}$

J.-C. Raut and  
P. Chazette

Title Page

Abstract

Introduction

Conclusions

References

Tables

Figures

⏪

⏩

◀

▶

Back

Close

Full Screen / Esc

Printer-friendly Version

Interactive Discussion



where  $k_2$ , independent of time, is given by the least-squares method as:

$$k_2 = \rho \cdot \frac{4}{3} \pi \cdot \left( \overline{\sigma_{\text{ext},355}}^T \cdot \overline{\sigma_{\text{ext},355}} \right)^{-1} \cdot \overline{\sigma_{\text{ext},355}}^T \cdot \overline{r^3} \quad (6)$$

with  $\overline{\sigma_{\text{ext},355}}^T$  representing transpose of the vector  $\overline{\sigma_{\text{ext},355}} = \begin{pmatrix} \overline{\sigma_{\text{ext},355}}^{(1)} \\ \vdots \\ \overline{\sigma_{\text{ext},355}}^{(i)} \\ \vdots \\ \overline{\sigma_{\text{ext},355}}^{(n)} \end{pmatrix}$ .

The dimension of  $\overline{\sigma_{\text{ext},355}}$  is  $n$  ( $i=1$  to  $n$ ) corresponding to the number of temporal samples. In all the experimental campaigns, measurements are recorded every minute.  $k_2$  represents the mean value over the considered experiment.

### 3.4 Correction of the relative humidity influence

A common feature of tropospheric aerosol particles is their ability to absorb water vapour, whose state is often represented as a function of relative humidity (RH). As RH increases, condensation of water vapor may take place on the aerosol scatterers depending on their chemical composition (Tang and Munkelwitz, 1993). This phenomenon leads to the effects of deliquescence (hygroscopic growth of aerosols), crystallisation, hysteresis and existence of metastable droplets. Apart from the change in size, hygroscopic aerosols experience a change in their refractive index and in several key optical properties (scattering and absorption coefficients, single scattering albedo, asymmetry parameter, and aerosol optical depth). Quantification of aerosol micro-physical and optical properties and their dependency on relative humidity is needed to reduce the large associated uncertainty (Penner et al., 1994). Hänel (1976) described

Title Page

Abstract

Introduction

Conclusions

References

Tables

Figures

⏪

⏩

◀

▶

Back

Close

Full Screen / Esc

Printer-friendly Version

Interactive Discussion

aerosol growth in parameterising particle radius and refractive index for wet particles:

$$r_w = r \cdot \left( \frac{1 - RH}{1 - RH_{ref}} \right)^{-\varepsilon} \quad (7)$$

$$n_w = n_{H_2O} + (n - n_{H_2O}) \cdot \left( \frac{r_w}{r} \right)^{-3} \quad (8)$$

The suffix  $w$  refers to wet conditions and RH is the relative humidity.  $r$  and  $n$  are the radius and the refractive index of aerosol particles, respectively, at  $RH = RH_{ref}$ , and  $n_{H_2O}$  is the refractive index of pure water. The coefficient  $\varepsilon$  depends on the considered type of aerosol. It is determined in this study from ISORROPIA model (Nenes et al., 1998; <http://nenes.eas.gatech.edu/ISORROPIA>) since growth curves of water mass condensed around the aerosol can be parameterised versus humidity. As a consequence,  $\varepsilon$  is determined as follows (e.g. Randriamiarisoa et al., 2006):

$$\varepsilon = -\frac{1}{3} \cdot \log \left( \frac{1 + \frac{m_{H_2O} \cdot \rho_{dry}}{m_{dry}}}{1 + \frac{m_{H_2O,ref} \cdot \rho_{dry}}{m_{dry}}} \right) \cdot \left( \log \left( \frac{1 - RH}{1 - RH_{ref}} \right) \right)^{-1} \quad (9)$$

$m_{H_2O}$  (respectively  $m_{H_2O,ref}$ ) is the mass of water at RH (resp.  $RH_{ref}$ ).  $m_{dry}$  and  $\rho_{dry}$  represent the mass and density of dry aerosol, respectively. The knowledge of  $r_w$  and  $n_w$  then allows the derivation of the wet scattering coefficient of the aerosol through Mie computations. In this study, ISORROPIA model was used to determine  $m_{H_2O}$  in a “reverse mode”, in which known quantities are temperature, RH and the aerosol phase concentrations of  $NH_3$ ,  $H_2SO_4$ , Na, HCl and  $HNO_3$  determined from ionic analyses on the chemical filters. Both states of aerosol were considered: the thermodynamically stable state, where salts precipitate once the aqueous phase becomes saturated, and the metastable state, where the aerosol is composed only of a supersaturated aqueous phase.

When using lidar to remotely sense properties in the boundary layer, an accurate description of this effect becomes important to avoid ambiguous interpretation of lidar

**Assessment of vertically-resolved  $PM_{10}$**

J.-C. Raut and P. Chazette

Title Page

Abstract

Introduction

Conclusions

References

Tables

Figures

⏪

⏩

◀

▶

Back

Close

Full Screen / Esc

Printer-friendly Version

Interactive Discussion



backscatter data (e.g. Chazette et al., 2005b). It is important to distinguish the contribution of aerosol concentration from that of water in the variations of the backscatter coefficient. In translating remotely sensed extinction coefficient into dry aerosol mass, RH needs to be considered. In our case, the RH profile has passed the deliquescence point on the 27 May 2005 during the LISAIR campaign. Hence a correction has been applied using the increasing branch of the hysteresis (Fig. 1a) so as to exclusively consider the dry aerosol mass of the particles.

Furthermore, the use of nephelometer measurements is problematic when RH of the environment has passed the deliquescence point since particles can exist on the upper branch of the hysteresis curve. In entering the nephelometer chamber, RH decreases generally down to 30–40% and the droplets reduce their size by evaporation of water but they can exist below the deliquescence point as metastable supersaturated solutions. Such situations were encountered during experiments conducted in winter and early spring, i.e. in Brétigny (MEAUVE campaign) and Palaiseau (during Parisfog campaign), where the outside RH was between 70 and 95%. Thus, the hysteresis cycle of RH for those aerosols has been retrieved from ISORROPIA model (Fig. 1b and c) and the upper part of the cycle (efflorescence curve) has been used to translate scattering coefficients measured by the nephelometer into dry scattering coefficients, which could be compared to TEOM measurements (Sect. 3.2).

In Fig. 1, particles show the hysteresis effect in the growth curve. Starting at low RH, the dry particles do not change their size substantially until they reach the deliquescence point (between 45% and 65%) and a solution droplet is formed. There is some degree of water uptake prior deliquescence, which is most probably caused by water adsorption on imperfection sites of the aerosol matrix (Gysel et al., 2002). A further increase of the RH leads to particle growth by condensation of water in accordance with Köhler theory. At decreasing RH, the droplets reduce their size by evaporation of water, pass the saturation point, and continue to evaporate in the supersaturated concentration region. These results are in agreement with experiments reported in the literature, generally for ammonium sulfate aerosol (Tang and Munkelwitz, 1993, 1994;

---

## Assessment of vertically-resolved $PM_{10}$

J.-C. Raut and  
P. Chazette

---

[Title Page](#)[Abstract](#)[Introduction](#)[Conclusions](#)[References](#)[Tables](#)[Figures](#)[Back](#)[Close](#)[Full Screen / Esc](#)[Printer-friendly Version](#)[Interactive Discussion](#)

Badger et al., 2006; Gysel et al., 2004). The crystallisation point as predicted by the model is very low ( $RH < 15\%$ ).

In urban and periurban conditions (Fig. 1a and c, respectively), the hysteresis cycles are very similar. The deliquescence point is found a bit larger in rural conditions.

The main salts formed together with the variations in RH are  $(\text{NH}_4)_2\text{SO}_4$  and  $\text{NH}_4\text{NO}_3$  during LISAIR (Fig. 1a) and Parisfog (Fig. 1c) campaigns. During this latter, a part of the salts formed is also constituted by  $\text{Na}_2\text{SO}_4$ . Conversely, during MEAUVE campaign in rural conditions (Fig. 1b), the main inorganic salts formed onto the aerosols are  $\text{Na}_2\text{SO}_4$  and  $\text{NH}_4\text{NO}_3$ . According to Tang (1996), the theoretical deliquescence points of these individual salts are 80% for  $(\text{NH}_4)_2\text{SO}_4$ , 62% for  $\text{NH}_4\text{NO}_3$  and 84% for  $\text{Na}_2\text{SO}_4$ . The predominance of  $\text{Na}_2\text{SO}_4$  salt in the rural location with a larger deliquescence point tends to explain the discrepancies observed between the different situations in Fig. 1. We have to bear in mind that ISORROPIA model does not take into account organic compounds that can also be soluble products. Besides, differences can occur between summer and winter situations. A bias is therefore expected on our calculations. Because hysteresis cycles are only used in this study for deriving corrections on scattering coefficients, this effect is assumed to be low.

## 4 Optical to mass relationship for different aerosol types

### 4.1 $k_1$ and $k_2$ retrievals

Simple linear relationships between  $\alpha_{\text{scat},700}$ , measured in real time by the nephelometer and corrected from the non-observed angles and RH, and  $\text{PM}_{10}$ , measured in real time with the TEOM, have been investigated during the different campaigns. Results are plotted in Fig. 2. Various patterns of particulate pollution in Paris area are considered. Figure 2a and b shows the correlations obtained in urban conditions, i.e. directly in Paris centre. The correlation is much better during LISAIR program (Fig. 2a) due to a considerable set of measurements. Despite the limited number of samples ana-

Title Page

Abstract

Introduction

Conclusions

References

Tables

Figures

⏪

⏩

◀

▶

Back

Close

Full Screen / Esc

Printer-friendly Version

Interactive Discussion

**Assessment of  
vertically-resolved  
PM<sub>10</sub>**J.-C. Raut and  
P. Chazette

Title Page

Abstract

Introduction

Conclusions

References

Tables

Figures

◀

▶

◀

▶

Back

Close

Full Screen / Esc

Printer-friendly Version

Interactive Discussion

lyzed in Fig. 2b, the slopes are in agreement:  $C_0$  is  $\sim 0.98(\pm 0.10) \text{ g m}^{-2}$  during LISAIR (Fig. 2a) and  $\sim 1.10(\pm 0.10) \text{ g m}^{-2}$  during ESQUIF in Paris (Fig. 2b). Two cases belong to the periurban situations: Parisfog in Palaiseau and ESQUIF in Saclay (respectively Fig. 2c and d). During Parisfog campaign, a high number of real time observations were performed, which leads to a very nice correlation between  $\alpha_{\text{scat},700}$  and  $\text{PM}_{10}$ . The corresponding slope ( $\sim 0.82 \pm 0.10 \text{ g m}^{-2}$ ) is lower than that retrieved in Paris. It is confirmed by the result obtained in Saclay with  $C_0 \sim 0.77 \pm 0.10 \text{ g m}^{-2}$ . It is worthy to notice that these campaigns were carried out during different seasons: in winter and early spring for Parisfog and in summer for ESQUIF. Regardless of the season, and therefore of the type of organic matter present in the particles, the similarities in  $C_0$  for polluted aerosols is remarkable given the possible discrepancies in aerosol size distributions and chemical composition. This result is in agreement with the conclusions of Carrico et al. (2003). Only one case (Brétigny during MEAUVE) has concerned a rural situation influenced by pollution in the Paris area. Scarce measurements were available, which can explain the poor correlation derived from the regression analysis in Fig. 2e. The slope  $C_0$  is smaller than in the previous cases ( $0.39 \text{ g m}^{-2}$ ) but was accompanied with a large uncertainty (25%). Thus, the results of this situation will not be used for optical to mass conversion purposes in Sect. 5.

The slopes  $C_0$  of optical to mass relationships obtained for the described situations encountered are given in Table 1, together with the corresponding values of single scattering albedo and Angström exponent. Urban aerosols are smaller ( $a \sim 2.02$ ) and more absorbing ( $\omega_{0,355} \sim 0.89$ ) than those presenting a rural origin. This is most likely due to the high proportion of small black carbon particles in Paris streets because of the importance of vehicle traffic and combustion processes. When getting away from Paris in direction of the suburbs, aerosols have time to gather chemical components and the developed coating shell increases their sizes. This result is also suggested by the values of  $r^3$  and  $\sigma_{\text{ext},355}$  averaged over the whole campaigns.  $r^3$  and  $\sigma_{\text{ext},355}$  have been computed from the knowledge of size distribution and complex refractive index. During LISAIR, Raut and Chazette (2007) have found a mean size distribution

---

**Assessment of  
vertically-resolved  
PM<sub>10</sub>**J.-C. Raut and  
P. Chazette

---

[Title Page](#)[Abstract](#)[Introduction](#)[Conclusions](#)[References](#)[Tables](#)[Figures](#)[⏪](#)[⏩](#)[◀](#)[▶](#)[Back](#)[Close](#)[Full Screen / Esc](#)[Printer-friendly Version](#)[Interactive Discussion](#)

with nucleation and accumulation modes. No coarse mode was observed. The modal radii were  $0.03\ \mu\text{m}$  and  $0.08\ \mu\text{m}$ , both having a geometric deviation of 1.5. 94% of particles were in the fine mode. During ESQUIF, Chazette et al. (2005b) reported a size distribution with two modes with corresponding modal radii of  $0.03\ \mu\text{m}$  and  $0.07\ \mu\text{m}$ , both having a standard geometric deviation of 1.5. The first mode represented 83% of the total number of particles. The corresponding complex refractive indices have been derived by Raut and Chazette (2008a) through a synergy between lidar and in situ measurements for aerosol located inside (resp. outside) Paris plume:  $1.51\text{--}0.017i$  (resp.  $1.55\text{--}0.013i$ ). In Brétigny, the size distribution looked like that retrieved during ESQUIF experiment but with a larger second modal radius ( $0.1\ \mu\text{m}$ ). The complex refractive index has been computed from chemical analysis and Lorentz-Lorenz formula:  $1.55\text{--}0.019i$ .

## 4.2 Comparison of the approaches and specific cross-section

Coefficients  $k_1$  and  $k_2$  have been calculated according to the two approaches described in Sects. 3.2 and 3.3. The value of the mean density  $\rho$  of aerosols in the boundary layer, predominantly of urban origin, was required for the calculation of  $k_2$ . Biomass burning and dust events, discussed in Sect. 5.3, were mostly found in the free troposphere during LISAIR experiment, except on 26 and 27 May 2005. Thus, the limited influence of biomass burning and dust plumes on regional pollution of Paris area, hence on the mass-scattering relationship in the boundary layer, justifies the use of a single density value for the size distributions in the boundary layer. We estimated mass of ions, organic compounds and black carbon using chemical analyses during the different campaigns. Retrieved density values are reported in Table 1, present a small variability ( $\sim 5\%$ ) and fall within the density range of urban pollution samples ( $1.54\text{--}1.77\ \text{g/cm}^3$ , e.g. McMurry et al., 2002).

The comparison of both methods provides excellent results within a discrepancy of 3%. The  $k_1$  and  $k_2$  coefficients are provided with a reasonable uncertainty for aerosols of urban and periurban origins ( $\sim 12\%$ ). This confirms that both methods are equivalent

---

**Assessment of  
vertically-resolved  
PM<sub>10</sub>**J.-C. Raut and  
P. Chazette

---

Title Page

Abstract

Introduction

Conclusions

References

Tables

Figures

⏪

⏩

◀

▶

Back

Close

Full Screen / Esc

Printer-friendly Version

Interactive Discussion

and that the simple linear empirical relationship defined in Sect. 3.2 is appropriate to retrieve PM from extinction coefficients retrieved by lidar profiles. In the rural location (Brétigny), the uncertainty on PM<sub>10</sub> was larger: 26%. The inverse of these coefficients is called the specific extinction cross-section at 355 nm:  $s_{\text{ext},355}$ . Mean values for the different cases have also been mentioned in Table 1.  $s_{\text{ext},355}$  was found to be  $\sim 4.5 \text{ m}^2/\text{g}$  for urban aerosols, and a bit larger for particles observed on a more rural area  $5.9\text{--}7.1 \text{ m}^2/\text{g}$ . This is in agreement with results described in many studies (Table 2). They generally exhibit values in the range from  $3.5$  to  $4.5 \text{ m}^2/\text{g}$  for fine urban aerosol and between  $4$  and  $6 \text{ m}^2/\text{g}$  for fine anthropogenic aerosols in a remote site. Notwithstanding, those results are generally expressed in terms of scattering specific cross-sections in the mid-visible, which can explain, via  $\omega_{0,355}$  and  $a$ , that our retrievals present slightly larger values. Another bias can be ascribed to the fact that the frequently used cut-off diameter in USA studies is  $2.5 \mu\text{m}$  instead of  $10 \mu\text{m}$ . Nevertheless, the specific cross-sections are very similar regardless of the measurement site and period. As a consequence,  $k_1$  and  $k_2$  values will be used in the next section to convert aerosol extinction coefficient retrieved from lidar signals inversion into PM<sub>10</sub> profiles. Indeed, extinction coefficients derived from nephelometer measurements are in very good agreement (5% discrepancy) with those retrieved by the lidar when shooting horizontally at the same altitude of the nephelometer ( $\sim 4 \text{ m}$  above ground level).

## 5 Spatiotemporal variability of PM<sub>10</sub> in the troposphere

### 5.1 Analysis of lidar vertical profiles

As mentioned in Sect. 2.2, the LAUVA system has been operated onboard a small personal vehicle, which permits a regional study of anthropogenic particles in urban environment. Two kinds of experiments have been performed during the LISAIR program in May 2005. The first one has been devoted to the study of the particulate gradient between the large southern suburb of Paris (Saclay or Palaiseau) and Paris



centre (city hall of Paris). For the second application, observations have been carried out along the Paris Peripherique, so as to identify the role of this latter in the production of anthropogenic aerosols.

*Lidar-derived aerosol extinction coefficient.* In both cases, the lidar signals have been calibrated, range-corrected, corrected from the overlap factor and inverted using a well-known method based on Bernoulli's differential form of the propagation equation (Klett, 1981). This approach relies on the assumption of a constant BER (backscatter-to-extinction) in the tropospheric column, that has been assessed to be  $\sim 0.011 \text{ sr}^{-1}$  at 355 nm during the campaign through an iterative method converging when the optical thickness retrieved by the lidar is equal to that of the sunphotometer (Chazette, 2003). The retrieved extinction coefficients have been corrected from hygroscopic growth when the RH profile has passed the deliquescence point: it was the case during the night between 26 and 27 May 2005: RH was larger than 65% at the surface and in a layer located between 2.5 and 3 km height. The corresponding correction factor has been calculated using the increasing branch of the hysteresis (Sect. 3.3) in order to deal only with the dry aerosol mass of the particles.

*Lidar-derived vertical structures.* Lidar profiles have generally been obtained during evening or night periods, allowing the detection of multiple layers: boundary layer, nocturnal layer, residual layers and elevated layers in the free troposphere. The distinction between the different scattering layers in terms of vertical structures has been done through an algorithm sensitive to vertical heterogeneities in particulate concentrations derived from lidar profiles. On each profile, the minimum of the vertical gradient in aerosol extinction coefficient is detected (Dupont et al., 1994; Flamant et al., 1997). This has been done through an analytic derivation of the second order polynomial function retrieved from least square mean method applied onto the extinction coefficient. Calculations are realized in a sliding window, whose size is close to the thickness of the analysed transition area. The accuracy on the layer altitudes is close to 30 m. This algorithm is then applied to the whole temporal series of measured lidar profiles.

---

**Assessment of  
vertically-resolved  
PM<sub>10</sub>**J.-C. Raut and  
P. Chazette

---

Title Page

Abstract

Introduction

Conclusions

References

Tables

Figures

⏪

⏩

◀

▶

Back

Close

Full Screen / Esc

Printer-friendly Version

Interactive Discussion

## 5.2 Local contributions in the boundary and residual layers

Once the various layers have been delimited, an appropriate specific cross-section is attributed for each of them, according to the study performed in Sect. 4.1. Paris turns out to be one of the greatest urbanized areas in Europe, located far from other big cities so that the signatures and origins of pollution are easier to determine. The application of specific cross-sections is function of the advection conditions. In nocturnal conditions in particular, as in the cases discussed below, only two layers are generally detected. A coefficient  $k_1=0.217\text{ g/m}^2$  typical for urban aerosols is applied in the boundary layer or nocturnal layer for pollutants emitted on the urban area or Paris Peripherique. A coefficient  $k_1=0.177\text{ g/m}^2$  typical for periurban aerosols is applied in the residual layers for particles that were emitted on the previous day and trapped in altitude during the erosion of the boundary layer in the evening.

Two transects between the southern suburbs (Palaiseau) and Paris centre have been carried out on the 24 and 25 May in nighttime conditions before the morning traffic starts (Figs. 3 and 4, respectively). Both cases highlight the presence of stable layers corresponding to the inversion layer trapping pollutants at low altitudes and the residual layer in altitude. The top of the stable nocturnal layer is between 300 and 400 m on the 24 May (Fig. 3b) and lower than 500 m on the 25 May (Fig. 4b). The altitude of the residual layer was higher on the 24 May (0.8–1.5 km) than on the 25 May (0.4–0.9 km). This can be ascribed to the higher temperatures observed on the 23 May ( $\sim 23^\circ\text{C}$ ) than on the 25 May ( $\sim 18^\circ\text{C}$ ) enabling a stronger development of the convective layer during the day and therefore a residual layer trapped at higher altitude in the evening. In these layers, mass concentrations are rather constant.  $\text{PM}_{10}$  values are reported in Table 3. Concentrations are very similar in the residual layer but important differences can be noticed in the nocturnal layer.  $\text{PM}_{10}$  values are  $\sim 8\text{ }\mu\text{g m}^{-3}$  on the 24 May, which is very similar to those derived from a transect carried out on the 26 May between Paris and Saclay (southern suburb of Paris) before traffic in nighttime conditions (Table 3).  $\text{PM}_{10}$  values are  $\sim 24\text{ }\mu\text{g m}^{-3}$  on the 25 May. This is principally

### Assessment of vertically-resolved $\text{PM}_{10}$

J.-C. Raut and  
P. Chazette

Title Page

Abstract

Introduction

Conclusions

References

Tables

Figures

⏪

⏩

◀

▶

Back

Close

Full Screen / Esc

Printer-friendly Version

Interactive Discussion

due to the lower height of the surface nocturnal layer, preventing dilution on the 25 May. Wind measurements performed from the sonic anemometer indicate very low winds on the 25 May ( $\sim 0.5 \text{ m s}^{-1}$ ), also suggesting weak dilution processes. Such a mass concentration is close to that obtained on the 25 May in a well-developed boundary layer during the transect Paris – Saclay (Table 3).

Two situations around the Paris ring before and during the morning traffic period on the 25 May are illustrated in Figs. 5 and 6, respectively. Together with the increasing activity of the automobile traffic on the morning, surface concentrations significantly rise by  $\sim 50\%$  between 05:00 and 08:00 UTC (Table 3). The slow development of the boundary layer, due to a low surface temperature ( $\sim 17^\circ\text{C}$ ), leads to a mixing of the layers containing residual pollutants with those recently emitted on the surface. Considering the factor 2 on the mass concentrations in the centre of Paris (from  $30 \text{ } \mu\text{g m}^{-3}$ ), the impact on air quality is clearly noticeable.

### 5.3 Role of the long-range transport

Such an increase of particulate concentrations in the lowest layers of the troposphere has also been observed on the 26 May in the evening (Fig. 7b). This phenomenon occurs after the formation of the nocturnal inversion trapping aerosols that are still emitted at this period in the centre of Paris (St. Michel district). We can also notice a plume in altitude aloft A6 highway in the South of Paris linked to particles emitted from automobile traffic a few hours before. This plume appears after the temperature inversion close to the ground and is associated with the nightfall. In addition to the nocturnal inversion layer and the residual layers, observations performed on 26 and 27 May (Figs. 7b and 8b) also highlight elevated layers from a different origin. Indeed, Paris agglomeration has a rather flat topography and is then also strongly influenced by synoptic meteorological conditions. Measurements performed in the vicinity of the city hall of Paris by LESAA lidar confirm those observations. Figure 9a presents the temporal evolution of these layers on the 26 May. The classical development of the boundary layer, its mixing with the elevated residual layer at  $\sim 12:00$  UTC, its erosion

**Assessment of  
vertically-resolved  
PM<sub>10</sub>**

J.-C. Raut and  
P. Chazette

Title Page

Abstract

Introduction

Conclusions

References

Tables

Figures

⏪

⏩

◀

▶

Back

Close

Full Screen / Esc

Printer-friendly Version

Interactive Discussion



in the evening, the development of the nocturnal layer and the corresponding accumulation of pollutants close to the surface are clearly visible on those lidar profiles. We can also notice that the top height of the planetary boundary layer (PBL) is maintained at a fairly constant level in the afternoon. It is due to an anticyclone located over central Europe than maintains high mean sea-level pressure over the Paris area (1015–1018 hPa) and hinders the development of the PBL.

The aerosol extinction coefficient nevertheless shows unexpected large values between ~2 and 4 km altitude all day long and higher values at ~3 km from 15:00 UTC. At this altitude, the aerosols are not characterized by a significant depolarization ratio, whereas the particles located in the highest layer present stronger depolarization ratios (~0.05), twice larger than the background level. Hence, aerosols within the highest layer could include a mineral contribution associated to non spherical particles whereas the aerosols located in the PBL and in the upper layer appear rather spherical. Such observations are in accordance with the fact that aerosols at ~3 km are rather biomass burning particles and those at ~4 km are dust particles.

The sources of biomass burning aerosols are likely forest fires in Portugal or Spain, accordingly to backtrajectories arriving over Paris on the 26 May at 20:00 UTC (Fig. 9c and d). These five-day backtrajectories of air masses were computed using the Hysplit model (courtesy of NOAA Air Resources Laboratory; <http://www.arl.noaa.gov>). This model uses the meteorological data to compute advection and dispersion of air parcels. Fire locations are given by MODIS (Moderate Resolution Imaging Spectroradiometer) fire products obtained from 21 to 24 May (Roy et al., 2005). Dry convective events can inject such primary aerosols of biomass smoke into the free troposphere especially during summer in Europe. Backtrajectories reaching Paris at 4 km suggest that aerosols in the highest layer may be nonspherical mineral dust coming from the Sahara and transported over the Atlantic Ocean. This is also in agreement with the simulations performed using the DREAM (Dust REgional Atmospheric Model) model (<http://www.bsc.es/projects/earthscience/DREAM/>).

These aerosols coming from Portugal, Spain or from the Sahara have different op-

---

## Assessment of vertically-resolved $PM_{10}$

J.-C. Raut and  
P. Chazette

---

[Title Page](#)[Abstract](#)[Introduction](#)[Conclusions](#)[References](#)[Tables](#)[Figures](#)[⏪](#)[⏩](#)[◀](#)[▶](#)[Back](#)[Close](#)[Full Screen / Esc](#)[Printer-friendly Version](#)[Interactive Discussion](#)

tical and microphysical properties than those retrieved in the vicinity of the surface from in situ measurements. In particular, lidar data inversion with the assumption of a constant BER would have lead to erroneous extinction coefficients, and therefore mass concentrations, in the dust layer. The BER profile has been corrected in this elevated layer to  $0.020 \text{ sr}^{-1}$ , while maintaining a constant BER value in the lowest layers ( $0.011 \text{ sr}^{-1}$ ), so as to converge towards the optical thickness given by the sunphotometer.

Given that there were not any direct mass to optics relationship available for biomass-burning and dust aerosols, the determination of  $\text{PM}_{10}$  concentrations in these layers has required the determination of  $k_2$ , through the knowledge of their corresponding size distributions and complex refractive indices. Concerning biomass-burning aerosols, a typical size distribution for particles observed in the Sahelian region has been retrieved from AERONET measurements performed in 2006 and 2007 in Banizoumbou (Raut and Chazette, 2008b). The number size distribution presents two modes with corresponding modal radii of  $0.07$  and  $0.69 \mu\text{m}$  with standard deviations of  $1.5$  and  $1.9$ , respectively. The first mode represents  $99\%$  of the total number of particles. The corresponding refractive index has been retrieved by Raut and Chazette (2008b) from a synergy between remote sensing and in situ measurements:  $1.53-0.047i$ . Concerning mineral dust particles transported from the Sahara to Western Europe, the size distribution is shifted towards the small radii during the transport. Thus, AERONET measurements performed between 1999 and 2008 over the stations of Paris, Palaiseau and Fontainebleau ( $48^\circ 24' 21'' \text{ N}$ ,  $2^\circ 42' 07'' \text{ E}$ ) have been used to extract typical size distributions for dust episodes observed over the Paris area selected by an Angström exponent (between  $400$  and  $670 \text{ nm}$ ) lower than  $0.8$  and a volume median radius larger than  $1.6 \mu\text{m}$ . The resulting size distribution presents three modes. The fine mode containing  $99.5\%$  of the number of aerosols has a modal radius of  $0.07 \mu\text{m}$  and a standard deviation of  $1.5$ . The second mode is located at  $0.63 \mu\text{m}$  with a geometric standard deviation of  $1.4$  and representing  $0.4\%$  of the number of aerosols. The third mode at  $1.96 \mu\text{m}$  with a standard deviation of  $1.7$  only stands for  $0.1\%$  in number concentration

**Assessment of  
vertically-resolved  
 $\text{PM}_{10}$** J.-C. Raut and  
P. Chazette

Title Page

Abstract

Introduction

Conclusions

References

Tables

Figures

⏪

⏩

◀

▶

Back

Close

Full Screen / Esc

Printer-friendly Version

Interactive Discussion

but represents a larger volume contribution. The complex refractive index of dust particles has been taken equal to  $1.52-0.007i$  from the results obtained over Niamey by Raut and Chazette (2008b).

The corresponding extinction cross-sections  $s_{\text{ext},355}$  are lower than those obtained for anthropogenic aerosols (Table 1):  $2.6 \text{ m}^2/\text{g}$  for biomass-burning particles and  $1.1 \text{ m}^2/\text{g}$  for mineral dust. The result for biomass-burning aerosols is in the range of values reported in the literature (Table 2) for fresh combustion aerosols (Reid et al., 2005) and over the South Western Iberia Peninsula (Pereira et al., 2008). The value of  $s_{\text{ext},355}$  retrieved for dust particles exported from Africa to Western Europe in this study is close to that found for aged dust over the Atlantic Ocean ( $1.1 \text{ m}^2/\text{g}$ ; Clarke et al., 1996), for dust in the South Western Iberia Peninsula ( $0.97 \text{ m}^2/\text{g}$ ; Pereira et al., 2008), and for dust transported over China ( $1.05 \pm 0.13 \text{ m}^2/\text{g}$ ; Alfaro et al., 2003). Notwithstanding, values are often found lower for dust (Table 2). This result indicates that aged dust particles have larger values of  $s_{\text{ext},355}$ . This is most likely because the aged dust has shifted to smaller sizes during transport, resulting in a smaller scattering cross-section (as  $r^2$ ) but also in a smaller mass (as  $r^3$ ), and therefore in a higher scattering efficiency (stronger  $s_{\text{ext},355}$ ).

The conversion of aerosol extinction coefficients into  $\text{PM}_{10}$  through the parameter  $k_2$  requires the detection of the top and bottom altitudes of layers transporting biomass-burning and dust aerosols. This has been done thanks to the algorithm based on the strongest gradient in aerosol concentrations, mentioned in Sect. 5.1. These altitudes also fit well to the variations observed in the mean profile of potential temperature drawn in Fig. 9b. The RH profile also presents significant variations along the vertical tropospheric column. RH is  $\sim 50\%$  in the atmospheric boundary layer (up to 1.2 km) but decreases down to 22% in the residual layer (up to 2.5 km), then sharply increases up to 80% in the more humid biomass-burning layer (2.5–3.2 km). The highest layer (3.5–4 km) containing mineral dust is relatively dry ( $\text{RH} < 55\%$ ). It is possible that this layer is composed by a mixing of dust and biomass-burning particles, but backtrajectories alone do not enable to conclude.

---

**Assessment of  
vertically-resolved  
 $\text{PM}_{10}$** J.-C. Raut and  
P. Chazette

---

Title Page

Abstract

Introduction

Conclusions

References

Tables

Figures

⏪

⏩

◀

▶

Back

Close

Full Screen / Esc

Printer-friendly Version

Interactive Discussion

**Assessment of  
vertically-resolved  
PM<sub>10</sub>**J.-C. Raut and  
P. Chazette

Title Page

Abstract

Introduction

Conclusions

References

Tables

Figures

⏪

⏩

◀

▶

Back

Close

Full Screen / Esc

Printer-friendly Version

Interactive Discussion

The resulting temporal evolutions of PM<sub>10</sub> vertical profile are shown in Fig. 7b during the Palaiseau-Paris transect on the 26 May in the evening and in Fig. 8b over the Paris Peripherique during the night from 26 to 27 May. Aerosol concentrations are more important on the 27 May ( $\sim 33 \mu\text{g m}^{-3}$ ) due to the low inversion layer preventing vertical dilution than on the 26 May in the afternoon ( $\sim 13 \mu\text{g m}^{-3}$ ). PM<sub>10</sub> in the residual layer are almost similar ( $6\text{--}11 \mu\text{g m}^{-3}$ ), although slightly larger in nighttime conditions. This approach also enables to clearly follow the spatiotemporal evolution on the biomass-burning aerosols mass concentration transported over Paris area from the South Western Iberia Peninsula. This episode occurs on the 26 May in the afternoon (Table 3) with low aerosol mass concentrations ( $\sim 9 \mu\text{g m}^{-3}$ ). In the evening, the aerosol loading is much more important ( $\sim 41 \mu\text{g m}^{-3}$ ) and turns out to be the predominant source of pollutants in mass in the troposphere (Fig. 7b). During the night from 26 to 27 May (Fig. 8b), this plume appears more diluted ( $\sim 28 \mu\text{g m}^{-3}$ ). Conversely, the dust layer stays very constant in terms of shape and aerosol loading during its transport over the Paris area (Table 3).

The knowledge of the vertical distribution of PM<sub>10</sub> in the various tropospheric layers is particularly crucial when surface concentrations are influenced by the subsidence of air masses from the elevated layers aloft the boundary layer. This phenomenon occurred on the 26 May at  $\sim 20:00$  UTC (22:00 local time). After the evening rush hour linked to the automobile traffic jam ( $\sim 17:00\text{--}18:00$  UTC), PM<sub>10</sub> concentrations measured at the surface by a TEOM of Paris air quality network (AIRPARIF, Les Halles station) were maintained at a fairly constant level ( $15\text{--}20 \mu\text{g m}^{-3}$ ). Between 19:00 and 20:00 UTC, PM<sub>10</sub> strongly increase by a factor 3 up to a level of  $45 \mu\text{g m}^{-3}$ . This sharp increase cannot be explained by the erosion of the boundary layer, which only decreases by a factor 1.8. A more plausible scenario is the subsidence of aerosols from the residual layers, followed by the incorporation of those particles in the boundary layer during the erosion of this latter. The lidar profiles on Fig. 9a tend to illustrate this likely hypothesis. An accurate knowledge of the vertical distribution of PM<sub>10</sub> would therefore be required in air quality models so as to more precisely follow the variations of aerosol



concentrations at the surface.

## 6 Discussion on retrieved mass concentrations

We evaluated the concentrations derived from mobile lidar measurements on AIR-  
PARIF air quality network stations. Figures 3a, 4a, 5a, 6a, 7a and 8a present the  
5 spatial distribution of the stations considered in this study together with  $PM_{10}$  concentrations reported from TEOM measurements at these stations. AIRPARIF observations are given each hour and are provided in this work at the nearest hour of lidar profiles. Lidar signals produce a sequence of analyzed states, which are thereafter compared to hourly observations through a statistical parameter: the statistical measure to evaluate  
10 the results is the Root Mean Square Error (RMSE), expressed in  $\mu\text{g m}^{-3}$ , defined by the geometric average of the differences between lidar-derived  $PM_{10}$  at 200 m above ground level and  $PM_{10}$  observations performed by AIRPARIF air quality network stations at the surface. In a general manner, a strong variability is observed in the concentrations measured by the lidar in the lowest layers of the boundary and nocturnal  
15 layers. The corresponding RMSE has been found to be  $\sim 14 \mu\text{g m}^{-3}$ , which is of the order of half the concentrations observed in the Paris area. We have to bear in mind that the natural temporal fluctuations of the  $PM_{10}$  values in Paris are characterized by a standard deviation of  $5 \mu\text{g m}^{-3}$  on a one-hour basis (retrieved from our continuous TEOM measurements). Besides, AIRPARIF stations are not exactly localized on the  
20 path used by the small vehicle embarking LAUVA lidar. The spatial variability of mass concentrations thus contributes to the global RMSE.

There is furthermore a possible discrepancy between the concentrations derived from the lidar at 200 m above ground level and concentrations reported by stations directly at the surface. In regional chemistry-transport models, the assumption of a  
25 well-mixed lowest layer is generally made down to the surface, enabling a direct comparison of surface concentrations and  $PM_{10}$  derived from remote sensing applications a few hundred meters above. This coarse hypothesis has been tested in this study

### Assessment of vertically-resolved $PM_{10}$

J.-C. Raut and  
P. Chazette

Title Page

Abstract

Introduction

Conclusions

References

Tables

Figures

⏪

⏩

◀

▶

Back

Close

Full Screen / Esc

Printer-friendly Version

Interactive Discussion





**Assessment of  
vertically-resolved  
PM<sub>10</sub>**J.-C. Raut and  
P. Chazette

Title Page

Abstract

Introduction

Conclusions

References

Tables

Figures

⏪

⏩

◀

▶

Back

Close

Full Screen / Esc

Printer-friendly Version

Interactive Discussion

from lidar measurements performed on the 12 July 2005 over Palaiseau under high aerosol loading: the optical thickness at 380 nm given by AERONET sunphotometer in Palaiseau was  $\sim 0.9$  and the corresponding Angström exponent between 440 and 670 nm was 1.6, indicating the presence of small aerosols. Multiangle lidar measurements were performed in the evening after 19:00 UTC in order to follow the erosion of the atmospheric boundary layer and the possible vertical particulate gradient close to the surface. Lidar measurements identified a Rayleigh zone above 1.5 km. This zone has been taken as a reference area to invert lidar signals with a BER of  $0.011 \text{ sr}^{-1}$ , except for profiles captured with a large zenithal angle ( $>68^\circ$ ): corresponding lidar signals indeed reach the Rayleigh zone for emitter-scatterers distances of the order of 4 km, i.e. at distances where signal-to-noise ratio is too weak to permit an inversion with a satisfying accuracy. As a consequence, lidar profiles with large zenithal angles have been inverted through a Klett method, choosing for reference aerosol extinction coefficients retrieved at 1 km altitude from lidar signals measured at lower zenithal angles. This approach assumes that the atmosphere is horizontally homogeneous over the explored angular range (Sicard et al., 2002). The reconstitution of the aerosol extinction coefficient has been done down to 5 m above the ground (zenithal angle of  $88^\circ$  and overlap factor at 150 m, Fig. 10).

This tomographic approach has enabled to follow the decreasing height of the aerosol layer against time: the top altitude of the layer was 1.2 km at 19:00 UTC, decreased down to 0.8 at 20:00 UTC and reached 0.6 at 21:00 UTC (Fig. 10). It has also highlighted a sharp increase in the extinction coefficient profile between the ground and the top of the aerosol layer. Therefore, this approach clearly underlines a strong decorrelation between observations at the surface and measurements performed at 200 m above ground level, as also highlighted by Chazette et al. (2005b) from airborne measurements performed over Paris area. According to this effect, the resulting RMSE of  $14 \mu\text{g m}^{-3}$  retrieved between lidar-derived PM<sub>10</sub> and observations realized at the surface is therefore not very important and suggests a good reliability of the approach developed in this study. Lidar signals can be used to follow mass concentrations at the

surface and provide useful information on PM<sub>10</sub> peak forecasting that affect air quality.

## 7 Conclusions

This study describes two approaches to convert vertical profiles of aerosol extinction coefficients retrieved from lidar measurements into mass concentrations in terms of PM<sub>10</sub> or PM<sub>2.5</sub>. Simple linear relationships between the scattering coefficient at 700 nm, continuously measured by a nephelometer and corrected from the non-observed angles and RH, and PM<sub>10</sub>, measured with a TEOM, have been investigated during various campaigns performed in the Paris area since 1999. The comparison between the theoretical approach, based on the mean least square method, and this empirical relationship provides excellent results within a discrepancy of 3%. Therefore, specific cross-sections at 355 nm are provided with a reasonable uncertainty for aerosols of urban and periurban origins (~12%). This confirms that both methods are equivalent and that the simple linear empirical relationship is appropriate to retrieve PM from extinction coefficients retrieved by lidar profiles. In a rural location, the uncertainty was found larger: 26%.

Once the various layers have been delimited through an algorithm sensitive to vertical heterogeneities derived from lidar profiles, an appropriate specific cross-section was attributed for each of them: 4.5 m<sup>2</sup>/g for urban aerosol, 5.9 m<sup>2</sup>/g in periurban conditions, 7.1 m<sup>2</sup>/g for rural particles. This study permits to assess the role of the Paris Peripherique in local particulate pollution and the horizontal gradient of pollution between Paris centre and its remote suburbs. In addition to the nocturnal inversion layer and the residual layers, observations performed in Paris also highlight elevated layers from a different origin biomass burning aerosols (2.6 m<sup>2</sup>/g) and mineral dust particles (1.1 m<sup>2</sup>/g). This approach enables to clearly follow the spatiotemporal evolution on the biomass-burning aerosols transported over Paris area from the South Western Iberia Peninsula, which can be the predominant source of pollutants in mass in the troposphere. Conversely, the dust layer stays very constant in terms of shape and aerosol

### Assessment of vertically-resolved PM<sub>10</sub>

J.-C. Raut and  
P. Chazette

Title Page

Abstract

Introduction

Conclusions

References

Tables

Figures

⏪

⏩

◀

▶

Back

Close

Full Screen / Esc

Printer-friendly Version

Interactive Discussion

loading during its transport over the Paris area. The knowledge of the vertical distribution of aerosols is important in case of air masses subsidence from the elevated layers inside the boundary layer.

Multiangular lidar measurements have highlighted a possible discrepancy between  $PM_{10}$  derived from the lidar at 200 m above ground level and concentrations reported by stations directly at the surface. The resulting RMSE between lidar-derived  $PM_{10}$  at 200 m above ground and surface network stations measurements was  $\sim 14 \mu g m^{-3}$ . This suggests a good reliability of the approach. Lidar signals can be used to follow mass concentrations at the surface and provide useful information on  $PM_{10}$  peak forecasting that affect air quality. Hence, lidar observations could be used to validate air quality models in terms of particulate pollution. Vertically resolved measurements in the atmospheric column are indeed required to get reliable forecasts. This paper enables to envisage improved decision-support tools based on assimilation approaches or ensemble analyses. On the long run, an assimilation of vertical profiles of mass concentrations provided by a lidar network could be considered to improve the description of the vertical mixing processes in the atmospheric column. This could be done by a sequential assimilation using an ensemble Kalman filter.

*Acknowledgements.* This LISAIR program was funded by the city hall of Paris and the Commissariat à l'Énergie Atomique (CEA).



The publication of this article is financed by CNRS-INSU.

13501

ACPD

9, 13475–13521, 2009

## Assessment of vertically-resolved $PM_{10}$

J.-C. Raut and  
P. Chazette

Title Page

Abstract

Introduction

Conclusions

References

Tables

Figures

⏪

⏩

◀

▶

Back

Close

Full Screen / Esc

Printer-friendly Version

Interactive Discussion



## References

- Adam, M., Pahlow, M., Kovalev, V. A., Ondov, J. M., Parlange, M. B., and Nair, N.: Aerosol optical characterization by nephelometer and lidar: The Baltimore Supersite experiment during the Canadian forest fire smoke intrusion, *J. Geophys. Res.*, 109, D16S02, doi:10.1029/2003JD004047, 2004.
- Alfaro, S. C., Gomes, L., Rajot, J. L., Lafon, S., Gaudichet, A., Chatenet, B., Maille, M., Cautenet, G., Lasserre, F., Cachier, H., and Zhang, X. Y.: Chemical and optical characterization of aerosols measured in spring 2002 at the ACE-Asia supersite, Zhenbeitai, China, *J. Geophys. Res.*, 108(D23), 8641, doi:10.1029/2002JD003214, 2003.
- Andreae, T. W., Andreae, M. O., Ichoku, C., Maenhaut, W., Cafmeyer, J., Karnieli, A., and Orlovsky, L.: Light scattering by dust and anthropogenic aerosol at a remote site in the Negev desert, Israel, *J. Geophys. Res.*, 107(D2), 4008, doi:10.1029/2001jd900252, 2002.
- Badger, C. L., George, I., Griffiths, P. T., Braban, C. F., Cox, R. A., and Abbatt, J. P. D.: Phase transitions and hygroscopic growth of aerosol particles containing humic acid and mixtures of humic acid and ammonium sulphate, *Atmos. Chem. Phys.*, 6, 755–768, 2006, <http://www.atmos-chem-phys.net/6/755/2006/>.
- Bergin, M. H., Cass, G. R., Xu, J., Fang, C., Zeng, L. M., Yu, T., Salmon, L. G., Kiang, C. S., Tang, X. Y., Zhang, Y. H., and Chameides, W. L.: Aerosol radiative, physical, and properties in Beijing during June, 1999, *J. Geophys. Res.*, 106, 17969–17980, 2001.
- Bodhaine, B. A., Ahlquist, N. C., and Schnell, R. C.: Threewavelength nephelometer suitable for aircraft measurements of background aerosol scattering coefficient, *Atmos. Environ.*, 10, 2268–2276, 1991.
- Cachier, H., Brémond, M. P., and Patrick, B. M.: Determination of atmospheric soot carbon with a simple thermal method, *Tellus*, 41B, 379–390, 1989.
- Carrico, C. M., Bergin, M. H., Xu, J., Baumann, K., and Maring, H.: Urban aerosol radiative properties: Measurements during the 1999 Atlanta Supersite Experiment, *J. Geophys. Res.*, 108(D7), 8422, doi:10.1029/2001JD001222, 2003.
- Chazette, P. and Lioussé, C.: A case study of optical and chemical apportionment for urban aerosols in Thessaloniki, *Atmos. Environ.*, 35, 2497–2506, 2001.
- Chazette, P., Pelon J., Moulin C., Dulac F., Carrasco I., Guelle W., Bousquet P., and Flamant P. H.: Airborne lidar and Meteosat synergy to characterize a Saharan dust plume over the Azores during SOFIA/ASTEX, *Atmos. Environ.*, 35, 4297–4304, 2001.

### Assessment of vertically-resolved PM<sub>10</sub>

J.-C. Raut and  
P. Chazette

Title Page

Abstract

Introduction

Conclusions

References

Tables

Figures

◀

▶

◀

▶

Back

Close

Full Screen / Esc

Printer-friendly Version

Interactive Discussion

**Assessment of  
vertically-resolved  
PM<sub>10</sub>**J.-C. Raut and  
P. Chazette

Title Page

Abstract

Introduction

Conclusions

References

Tables

Figures

◀

▶

◀

▶

Back

Close

Full Screen / Esc

Printer-friendly Version

Interactive Discussion

- Chazette, P.: The monsoon aerosol extinction properties at Goa during INDOEX as measured with lidar, *J. Geophys. Res.*, 108(D6), 4187, doi:10.1029/2002JD002074, 2003.
- Chazette, P., Couvert, P., Randriamiarisoa, H., Sanak, J., Bonsang, B., Moral, P., Berthier, S., Salanave, S., and Toussaint, F.: Three-dimensional survey of pollution during winter in French Alps valleys, *Atmos. Environ.*, 39, 1035–1047, 2005a.
- Chazette, P., Randriamiarisoa, H., Sanak, J., Couvert, P., and Flamant, C.: Optical properties of urban aerosol from airborne and ground based in situ measurements performed during the ESQUIF program, *J. Geophys. Res.*, 110, D02206, doi:10.1029/2004JD004810, 2005b.
- Chazette, P., Sanak, J., and Dulac, F.: New Approach for Aerosol Profiling with a Lidar Onboard an Ultralight Aircraft: Application to the African Monsoon Multidisciplinary Analysis, *Environ. Sci. Technol.*, 41, 8335–8341, 2007.
- Chu, D. A., Kaufman, Y. J., Zibordi, G., Chern, J. D., Mao, J., Li, C., and Holben, B. N.: Global monitoring of air pollution over land from the Earth observing System-Terra Moderate Resolution Imaging Spectroradiometer (MODIS), *J. Geophys. Res.*, 108(D21), 4661, doi:10.1029/2002JD003179, 2003.
- Clarke, A. D., Porter, J. N., Valero, F. P. J., and Pilewskie, P.: Vertical profiles, aerosol microphysics, and optical closure during the Atlantic Stratocumulus Transition Experiment: Measured and modeled column optical properties, *J. Geophys. Res.*, 101, 4443–4453, 1996.
- Dockery, D. and Pope, A.: Epidemiology of acute health effects: summary of time-series, in: *Particles in Our Air: Concentration and Health Effects*, edited by: Wilson, R. and Spengler, J. D., Harvard University Press, Cambridge, MA, USA, 123–147, 1996.
- Donaldson, K., Li, X. Y., and MacNee, W.: Ultrafine (nanometer) particle mediated lung injury, *J. Aerosol Sci.*, 29, 553–560, 1998.
- Dupont, E., Pelon, J., and Flamant, C.: Study of the moist Convective Boundary Layer structure by backscattering lidar, *Bound.-Lay. Meteorol.*, 69, 1–25, 1994.
- Dzubay, T. G., Stevens, R. K., Lewis, C. W., Hern, D. H., Courtney, W. J., Tesch, J. W., and Mason, M. A.: Visibility and aerosol composition in Houston, Texas, *Environ. Sci. Technol.*, 16, 514–525, 1982.
- Elias, T., Haeffelin, M., Drobinski, P., Gomes, L., Rangognio, J., Bergot, T., Chazette, P., Raut, J.-C., and Coulomb, M.: Particulate contribution to extinction of visible radiation: pollution, haze, and fog, *Atmos. Res.*, 92(4), 443–454, doi:10.1016/j.atmosres.2009.01.006, 2009.
- Flamant, C., Pelon, J., Flamant, P. H., and Durand, P.: Lidar determination of the entrainment zone thickness at the top of the unstable marine atmospheric boundary-layer, *Bound.-Lay.*

**Assessment of  
vertically-resolved****PM<sub>10</sub>**J.-C. Raut and  
P. Chazette

Title Page

Abstract

Introduction

Conclusions

References

Tables

Figures

⏪

⏩

◀

▶

Back

Close

Full Screen / Esc

Printer-friendly Version

Interactive Discussion

Meteorol., 83, 247–284, 1997.

Gysel, M., Weingartner, E., and Baltensperger, U.: Hygroscopicity of aerosol particles at low temperatures, 2. Theoretical and experimental hygroscopic properties of laboratory generated aerosols, *Environ. Sci. Technol.*, 36, 63–68, 2002.

5 Gysel, M., Weingartner, E., Nyeki, S., Paulsen, D., Baltensperger, U., Galambos, I., and Kiss, G.: Hygroscopic properties of water-soluble matter and humic-like organics in atmospheric fine aerosol, *Atmos. Chem. Phys.*, 4, 35–50, 2004,  
<http://www.atmos-chem-phys.net/4/35/2004/>.

10 Haefelin, M., Bergot, T., Elias, T., Tardif, R., Carrer, D., Chazette, P., Colomb, M., Drobinski, P., Dupont, E., Dupont, J.-C., Gomes, L., Musson-Genon, L., Pietras, C., Plana-Fattori, A., Protat, A., Rangognio, J., Raut, J.-C., Rémy, S., Richard, D., Sciare, J., and Zhang, X.: PARISFOG, shedding new light on fog physical processes, *B. Am. Meteorol. Soc.*, in review, 2009.

15 Hänel, G.: The properties of atmospheric aerosol particles as functions of the Relative humidity at thermodynamic equilibrium with the surrounding moist air, *Adv. Geophys.*, 19, 73–188, 1976.

Hegg, D. A., Hobbs, P. V., Ferek, R. J., and Waggoner, A. P.: Measurements of some aerosol properties relevant to radiative forcing on the east coast of the United States, *J. Appl. Meteorol.*, 34, 2306–2315, 1995.

20 Hegg, D. A., Livingston, J., Hobbs, P. V., Novakov, T., and Russell, P.: Chemical apportionment of aerosol column optical depth off the mid-Atlantic coast of the United States, *J. Geophys. Res.*, 102, 25293–25303, 1997.

25 Hodzic, A., Vautard, R., Chazette, P., Menut, L., and Bessagnet, B.: Aerosol chemical and optical properties over the Paris area within ESQUIF project, *Atmos. Chem. Phys.*, 6, 3257–3280, 2006,  
<http://www.atmos-chem-phys.net/6/3257/2006/>.

Hoff, R. M., Guise-Bagley, L., Staebler, R. M., Wiebe, H. A., Brook, J., Georgi, B., and Dürsterdiek, T.: Lidar, nephelometer, and in situ aerosol experiments in southern Ontario, *J. Geophys. Res.*, 101(D14), 19199–19209, 1996.

30 Holben, B. N., Eck, T. F., Slutsker, I., et al.: AERONET – A federated instrument network and data archive for aerosol characterisation, *Remote Sens. Environ.*, 66, 1–16, 1998.

Ichoku, C., Andreae, M. O., Andreae, T. W., Meixner, F. X., Schebeske, G., Formenti, P., Maenhaut, W., Cafmeyer, J., Karnieli, A., and Orlovsky, L.: Interrelationships between aerosol

- characteristics and light scattering in an eastern Mediterranean arid environment, *J. Geophys. Res.*, 104, 24371–24393, 1999.
- Kambezidis, H. D., Peppes, A. A., and Melas, D.: An environmental experiment over Athens urban area under sea breeze conditions, *Atmos. Res.*, 36, 139–156, 1995.
- 5 Keskinen, J., Pietarinen, K., and Lehtimäki, M.: Electrical Low Pressure Impactor, *J. Aerosol Sci.*, 23(4), 353–360, 1992.
- Klett, J. D.: Stable analytical inversion solution for processing lidar returns, *Appl. Optics*, 20, 211–220, 1981.
- Koloutsou-Vakakis, S., Carrico, C. M., Kus, P., Rood, M. J., Li, Z., Shrestha, R., Ogren, J. A.,  
10 Chow, J. C., and Watson, J. G.: Aerosol properties at a midlatitude Northern Hemisphere continental site, *J. Geophys. Res.* 106(D3), 3019–3032, 2001.
- Landulfo, E., Papayannis, A., Artaxo, P., Castanho, A. D. A., de Freitas, A. Z., Souza, R. F., Vieira Junior, N. D., Jorge, M. P. M. P., Sánchez-Ccoyllo, O. R., and Moreira, D. S.: Synergetic measurements of aerosols over So Paulo, Brazil using LIDAR, sunphotometer and satellite data during the dry season, *Atmos. Chem. Phys.*, 3, 1523–1539, 2003,  
15 <http://www.atmos-chem-phys.net/3/1523/2003/>.
- Lavigne, C., Roblin, A., Chervet, P., and Chazette, P.: Experimental and theoretical studies of the aureole about a point source that is due to atmospheric scattering in the middle ultraviolet, *Appl. Optics*, 44, p. 1250, 2005.
- 20 Li, X., Maring, H., Savoie, D., Voss, K., and Prospero, J. M.: Dominance of mineral dust in aerosol light-scattering in the North Atlantic trade winds, *Nature*, 380, 416–419, 1996.
- Liu, Y., Park, R. J., Jacob, D. J., Li, Q., Kilaru, V., and Sarnat, J. A.: Mapping annual mean ground-level PM<sub>2.5</sub> concentrations using multiangle imaging spectroradiometer aerosol optical thickness over the contiguous united states, *J. Geophys. Res.*, 109, D22206, doi:10.1029/2004jd005025, 2004.  
25
- Lurmann, F. W., Wexler, A. S., Pandis, S. N., Musarra, S., Kumar, N., and Seinfeld, J. H.: Modeling urban and regional aerosols: II. Application to California's South coast air basin, *Atmos. Environ.*, 31, 2695–2715, 1997.
- McMurry, P. H., Wang, X., Park, K., and Ehara, K.: The relationship between mass and mobility for atmospheric particles: A new technique for measuring particle density, *Aerosol Sci. Tech.*, 36, 227–238, 2002.  
30
- Menut, L., Vautard, R., Flamant, C., Abonnel, C., Beekmann, M., Chazette, P., Flamant, P. H., Gombert, D., Guédalia, D., Kley, D., Lefebvre, M. P., Lossec, B., Martin, D., Mégie, G., Perros,

---

**Assessment of  
vertically-resolved  
PM<sub>10</sub>**J.-C. Raut and  
P. Chazette

---

Title Page

Abstract

Introduction

Conclusions

References

Tables

Figures

◀

▶

◀

▶

Back

Close

Full Screen / Esc

Printer-friendly Version

Interactive Discussion



**Assessment of  
vertically-resolved  
PM<sub>10</sub>**J.-C. Raut and  
P. Chazette

Title Page

Abstract

Introduction

Conclusions

References

Tables

Figures

⏪

⏩

◀

▶

Back

Close

Full Screen / Esc

Printer-friendly Version

Interactive Discussion

P., Sicard, M., and Toupance, G.: Measurements and modelling of atmospheric pollution over the Paris area: an overview of the ESQUIF Project, *Ann. Geophys.*, 18, 1467–1481, 2000, <http://www.ann-geophys.net/18/1467/2000/>.

Mestayer, P. and Coll, I.: The Urban Boundary Layer Field experiment over Marseille UBL/CLU-  
Escompte: Experimental set-up and first results, *Bound.-Lay. Meteorol.*, 114, 315–365,  
2005.

Nenes, A., Pandis, S. N., and Pilinis, C.: ISORROPIA: A new thermodynamic equilibrium model for multiphase multicomponent inorganic aerosols, *Aquat. Geochem.*, 4, 123–152, 1998.

Parkhurst, W. J., Tanner, R. L., Weatherford, F. P., Valente, R. J., and Meagher, J. F.: Historic  
PM<sub>2.5</sub>/PM<sub>10</sub> concentrations in the southeastern United States - Potential implications of the  
revised particulate matter standard, *J. Air Waste Manage.*, 49, 1060–1067, 1999.

Pelletier, B., Santer, R., and Vidot, J.: Retrieving of particulate matter from optical  
measurements: A semiparametric approach, *J. Geophys. Res.*, 112, D06208,  
doi:10.1029/2005JD006737, 2007.

Penner, J. E., Charlson, R. J., Hales, J. M., Laulainen, N. S., Leifer, R., Novakov, T., Ogren,  
J., Radke, L. F., Schwartz, S. E., and Travis, L.: Quantifying and minimizing uncertainty of  
climate forcing by anthropogenic aerosols, *B. Am. Meteorol. Soc.*, 75, 375–400, 1994.

Pereira, S., Wagner, F., and Silva, A. M.: Scattering properties and mass concentration of  
local and long-range transported aerosols over the South Western Iberia Peninsula, *Atmos.  
Environ.*, 42, 7623–7631, 2008.

Randriamiarisoa, H., Chazette, P., Couvert, P., Sanak, J., and Mégie, G.: Relative humidity  
impact on aerosol parameters in a Paris suburban area, *Atmos. Chem. Phys.*, 6, 1389–  
1407, 2006,  
<http://www.atmos-chem-phys.net/6/1389/2006/>.

Raut, J.-C. and Chazette, P.: Retrieval of aerosol complex refractive index from a synergy  
between lidar, sunphotometer and in situ measurements during LISAIR experiment, *Atmos.  
Chem. Phys.*, 7, 2797–2815, 2007,  
<http://www.atmos-chem-phys.net/7/2797/2007/>.

Raut, J.-C. and Chazette, P.: Vertical profiles of urban aerosol complex refractive index in the  
frame of ESQUIF airborne measurements, *Atmos. Chem. Phys.*, 8, 901–919, 2008a,  
<http://www.atmos-chem-phys.net/8/901/2008/>.

Raut, J.-C. and Chazette, P.: Radiative budget in the presence of multi-layered aerosol struc-  
tures in the framework of AMMA SOP-0, *Atmos. Chem. Phys.*, 8, 6839–6864, 2008b,



**Assessment of  
vertically-resolved  
PM<sub>10</sub>**J.-C. Raut and  
P. Chazette

Title Page

Abstract

Introduction

Conclusions

References

Tables

Figures

⏪

⏩

◀

▶

Back

Close

Full Screen / Esc

Printer-friendly Version

Interactive Discussion

<http://www.atmos-chem-phys.net/8/6839/2008/>.

Raut, J.-C., Chazette, P., and Fortain, A.: New approach using lidar measurements to characterize spatiotemporal aerosol mass distribution in an underground railway station in Paris, *Atmos. Environ.*, 43(3), 575–583, 2009.

Reid, J. S., Eck, T. F., Christopher, S. A., Koppmann, R., Dubovik, O., Eleuterio, D. P., Holben, B. N., Reid, E. A., and Zhang, J.: A review of biomass burning emissions part III: intensive optical properties of biomass burning particles, *Atmos. Chem. Phys.*, 5, 827–849, 2005, <http://www.atmos-chem-phys.net/5/827/2005/>.

Roy, D. P., Jin, Y., Lewis, P. E., and Justice, C. O.: Prototyping a global algorithm for systematic fire affected area mapping using MODIS time series data, *Remote Sens. Environ.*, 97, 137–162, 2005.

Shinozuka, Y., Clarke, A. D., Howell, S. G., Kapustin, V. N., McNaughton, C. S., Zhou, J., and Anderson, B. E.: Aircraft profiles of aerosol microphysics and optical properties over North America: Aerosol optical depth and its association with PM<sub>2.5</sub> and water uptake, *J. Geophys. Res.*, 112, D12S20, doi:10.1029/2006JD007918, 2007.

Sicard, M., Chazette, P., Pelon, J., Won, J. G., and Yoon, S. C.: Variational method for the retrieval of the optical thickness and the backscatter coefficient from multiangle lidar profiles, *Appl. Optics*, 41, 493–502, 2002.

Tang, I. N. and Munkelwitz, H. R.: Composition and temperature dependence of the deliquescence properties of hygroscopic aerosols, *Atmos. Environ.*, 27A, 467–473, 1993.

Tang, I. N. and Munkelwitz, H. R.: Water activities, densities, and refractive indices of aqueous sulfates and sodium nitrate droplets of atmospheric importance, *J. Geophys. Res.*, 99, 18801–18808, 1994.

Tang, I. N.: Chemical and size effects of hygroscopic aerosols on light scattering coefficient, *J. Geophys. Res.*, 101, 19245–19250, 1996.

Tombette, M., Chazette, P., Sportisse, B., and Roustan, Y.: Simulation of aerosol optical properties over Europe with a 3-D size-resolved aerosol model: comparisons with AERONET data, *Atmos. Chem. Phys.*, 8, 7115–7132, 2008, <http://www.atmos-chem-phys.net/8/7115/2008/>.

Trentmann, J., Andreae, M. O., Graf, H.-F., Hobbs, P. V., Ottmar, R. D., and Trautmann, T.: Simulation of a biomass-burning plume: Comparison of model results with observations, *J. Geophys. Res.*, 107(D2), 4013, doi:10.1029/2001jd000410, 2002.

van Donkelaar, A., Martin, R. V., and Park, R. J.: Estimating ground-level PM<sub>2.5</sub> using aerosol

optical depth determined from satellite remote sensing, *J. Geophys. Res.*, 111, D21201, doi:10.1029/2005JD006996, 2006.

Vautard, R., Menut, L., Beekmann, M., Chazette, P., Flamant, P. H., Gombert, D., Guédalia, D., Kley, D., Lefebvre, M.-P., Martin, D., Mégie, G., Perros, P., and Toupance, G.: A synthesis of the Air Pollution Over the Paris Region (ESQUIF) field campaign, *J. Geophys. Res.*, 108(D17), 8558, doi:10.1029/2003JD003380, 2003.

Vrekoussis, M., Liakakou, E., Koçak, M., Kubilay, N., Oikonomou, K., Sciare, J., and Mihalopoulos, N.: Seasonal variability of optical properties of aerosols in the Eastern Mediterranean M., *Atmos. Environ.*, 39, 7083–7094, 2005.

Waggoner, A. P., Weiss, A. P., Ahlquist, N. C., Covert, D. S., and Charlson, R. J.: Optical characteristics of atmospheric aerosols, *Atmos. Environ.*, 15, 1891–1909, 1981.

Wang, J. and Christopher, S. A.: Intercomparison between satellite-derived aerosol optical thickness and  $PM_{2.5}$  mass: implications for air quality studies, *Geophys. Res. Lett.*, 30(21), 2095, doi:10.1029/2003GL018174, 2003.

White, W. H., Macias, E. S., Nininger, R. C., and Schorran, D.: Size-resolved measurements of light scattering by ambient particles in the Southwestern USA, *Atmos. Environ.*, 28, 909–921, 1994.

**Assessment of  
vertically-resolved  
 $PM_{10}$**

J.-C. Raut and  
P. Chazette

Title Page

Abstract

Introduction

Conclusions

References

Tables

Figures

⏪

⏩

◀

▶

Back

Close

Full Screen / Esc

Printer-friendly Version

Interactive Discussion

## Assessment of vertically-resolved PM<sub>10</sub>

J.-C. Raut and  
P. Chazette

**Table 1.** Optical and microphysical parameters of different types of aerosols enabling the retrieval of specific extinction cross-sections.

Aerosol type	$C_0$ ( $10^{-1} \times \text{g/m}^2$ )	$\omega_{0.355}$	$a$	$k_1$ ( $10^{-1} \times \text{g/m}^2$ )	$\rho$ ( $\text{g/cm}^3$ )	$r^3$ ( $\text{m}^3$ )	$\sigma_{\text{ext},355}$ ( $\text{m}^2$ )	$k_2$ ( $10^{-1} \times \text{g/m}^2$ )	$S_{\text{ext},355}$ ( $\text{m}^2/\text{g}$ )
Urban	9.81	0.89	2.07	2.17	1.77	$1.18 \times 10^{-4}$	$3.96 \times 10^{-11}$	2.20	4.5
Periurban	8.21	0.93	2.15	1.77	1.68	$1.69 \times 10^{-4}$	$6.98 \times 10^{-11}$	1.71	5.9
Rural	3.86	0.91	1.36	1.40	1.67	$3.62 \times 10^{-4}$	$1.83 \times 10^{-10}$	1.38	7.1
Biomass burning	–	0.77	1.74	–	$\sim 2.00$	$1.64 \times 10^{-3}$	$3.54 \times 10^{-10}$	3.90	2.6
Dust	–	0.94	$\sim 0.8$	–	$\sim 2.00$	$7.03 \times 10^{-3}$	$6.72 \times 10^{-10}$	8.76	1.1

[Title Page](#)
[Abstract](#)
[Introduction](#)
[Conclusions](#)
[References](#)
[Tables](#)
[Figures](#)
[Back](#)
[Close](#)
[Full Screen / Esc](#)
[Printer-friendly Version](#)
[Interactive Discussion](#)

**Table 2.** Specific scattering cross-sections for different types of aerosols reported in the literature.

Aerosol type	Specific scattering cross-section (m <sup>2</sup> /g)	Location	References
Fine PM, Urban	3.1±0.2	New York City (USA)	Waggoner et al. (1981)
	3.5	Houston (USA)	Dzubay et al. (1982)
	2.4–2.5	Southwest USA	White et al. (1994)
	3.2	NE Atlantic	Hegg et al. (1995)
	4.0±0.7	NE Atlantic	Clarke et al. (1996)
	3.2	Ontario, Canada	Hoff et al. (1996)
	2.8	Mid-atlantic coast, USA	Hegg et al. (1997)
	2.3–6	Beijing, China	Bergin et al. (2001)
	2.65	Tessaloniki, Grece	Chazette and Liousse (2001)
	4.10–4.57	Bondville, USA	Koloutsou-Vakakis et al. (2001)
	3.5–4.4	Atlanta, USA	Carrico et al. (2003)
Fine PM, remote site	4.55	South Western Iberia Peninsula	Pereira et al. (2008)
	3.7±0.6	Negev desert, Israël	Ichoku et al. (1999)
	5.8±0.2	Negev desert, Israël	Andreae et al. (2002)
Biomass burning	5.6–5.9	Eastern Mediterranean	Vrekoussis et al. (2005)
	4.06	Simulation (Mie)	Trentmann et al. (2002)
	0.2–3.3	Baltimore, Canada	Adam et al. (2004)
	2.8–4.2	Fresh aerosol (review)	Reid et al. (2005)
	3.5–4.2	Aged aerosol (review)	
Dust	2.48	South Western Iberia Peninsula	Pereira et al. (2008)
	0.34–0.45	Southwest, USA	White et al. (1994)
	1.1	Aged dust, Atlantic Ocean	Clarke et al. (1996)
	0.83	Aged dust, Barbados	Li et al. (1996)
	0.71±0.04	Negev desert, Israël	Andreae et al. (2002)
	1.05±0.13	Transported dust, China	Alfaro et al. (2003)
	0.21–0.96	Eastern Mediterranean	Vrekoussis et al. (2005)
0.97	South Western Iberia Peninsula	Pereira et al. (2008)	

## Assessment of vertically-resolved PM<sub>10</sub>

J.-C. Raut and  
P. Chazette

Title Page

Abstract

Introduction

Conclusions

References

Tables

Figures

◀

▶

◀

▶

Back

Close

Full Screen / Esc

Printer-friendly Version

Interactive Discussion

## Assessment of vertically-resolved PM<sub>10</sub>

J.-C. Raut and  
P. Chazette

Title Page

Abstract

Introduction

Conclusions

References

Tables

Figures

⏪

⏩

◀

▶

Back

Close

Full Screen / Esc

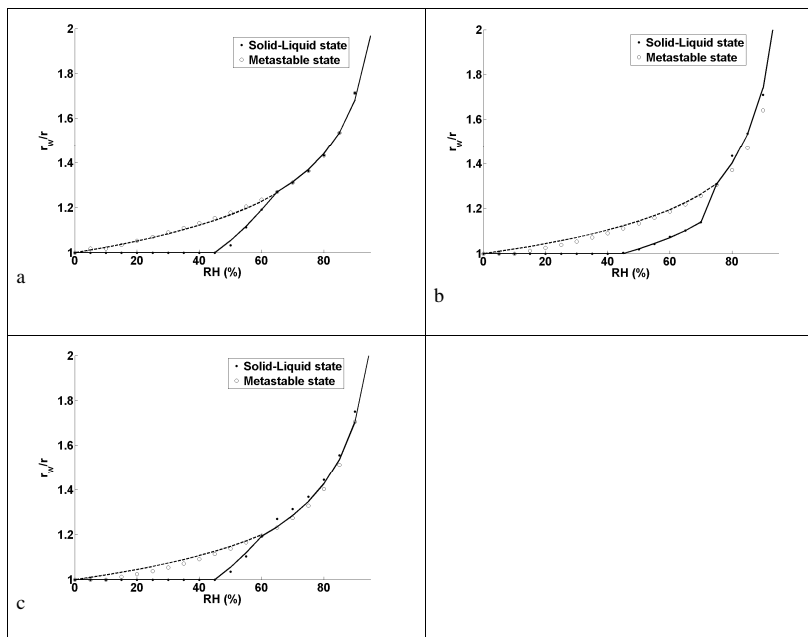
Printer-friendly Version

Interactive Discussion



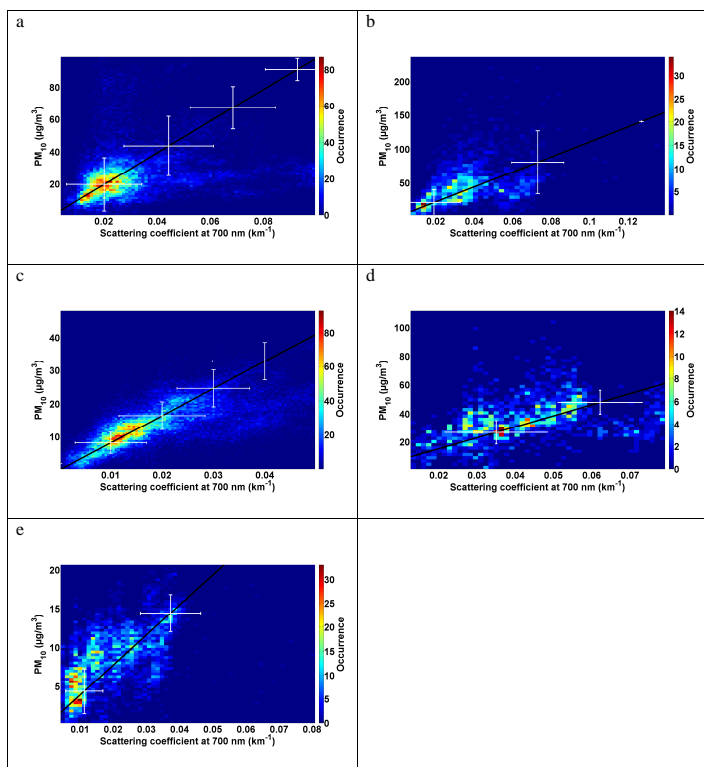
**Table 3.** Mean mass concentrations in terms of PM<sub>10</sub> values and associated standard deviations in layers detected from the mobile lidar during the LISAIR campaign over the Paris area.

Date Location	Diurnal/Nocturnal Conditions	Figure	PM <sub>10</sub> (μg/m <sup>3</sup> ) 1st layer	PM <sub>10</sub> (μg/m <sup>3</sup> ) 2nd layer	PM <sub>10</sub> (μg/m <sup>3</sup> ) 3rd layer	PM <sub>10</sub> (μg/m <sup>3</sup> ) 4th layer
24 May Palaiseau-Paris	Nighttime Before traffic	Fig. 3	8±3	10±11	–	–
25 May Palaiseau-Paris	Nighttime Before traffic	Fig. 4	24±5	11±10	–	–
25 May Paris	Nighttime Before traffic	Fig. 5	32±16	10±11	–	–
25 May Paris	Nighttime Traffic conditions	Fig. 6	46±41	17±12	–	–
25 May Paris-Saclay	Daytime Boundary layer well developed	–	24±16	–	–	–
26 May Paris-Saclay	Nighttime Before traffic	–	8±6	–	–	–
26 May Paris	Daytime Afternoon	–	18±6	3±3	9±14	17±26
26 May Palaiseau-Paris	Daytime Evening	Fig. 7	13±6	6±3	41±32	13±18
27 May Paris	Nighttime Before traffic	Fig. 8	33±25	11±5	28±20	10±15

**Assessment of  
vertically-resolved  
PM<sub>10</sub>**J.-C. Raut and  
P. Chazette

**Fig. 1.** Hysteresis cycle of phase transformation, growth and evaporation of aerosols derived from ISORROPIA model as a function of RH at ambient temperature in Paris during LISAIR **(a)**, in Brétigny during MEAUVE **(b)** and in Palaiseau during PARISFOG **(c)**.

[Title Page](#)[Abstract](#)[Introduction](#)[Conclusions](#)[References](#)[Tables](#)[Figures](#)[◀](#)[▶](#)[◀](#)[▶](#)[Back](#)[Close](#)[Full Screen / Esc](#)[Printer-friendly Version](#)[Interactive Discussion](#)

Assessment of  
vertically-resolved  
PM<sub>10</sub>J.-C. Raut and  
P. Chazette

**Fig. 2.** Correlations between the aerosol scattering coefficient at 700 nm measured by the nephelometer and PM<sub>10</sub> concentrations measured by the TEOM in urban conditions in Paris during LISAIR **(a)** and ESQUIF **(b)**, in periurban conditions in Palaiseau during PARISFOG **(c)** and in Saclay during ESQUIF **(d)**, and in rural conditions in Brétigny during MEAUVE **(e)**. White horizontal and vertical bars represent the corresponding standard deviations in terms of scattering coefficient and PM<sub>10</sub>, respectively.

[Title Page](#)[Abstract](#)[Introduction](#)[Conclusions](#)[References](#)[Tables](#)[Figures](#)[⏪](#)[⏩](#)[◀](#)[▶](#)[Back](#)[Close](#)[Full Screen / Esc](#)[Printer-friendly Version](#)[Interactive Discussion](#)

## Assessment of vertically-resolved $PM_{10}$

J.-C. Raut and  
P. Chazette

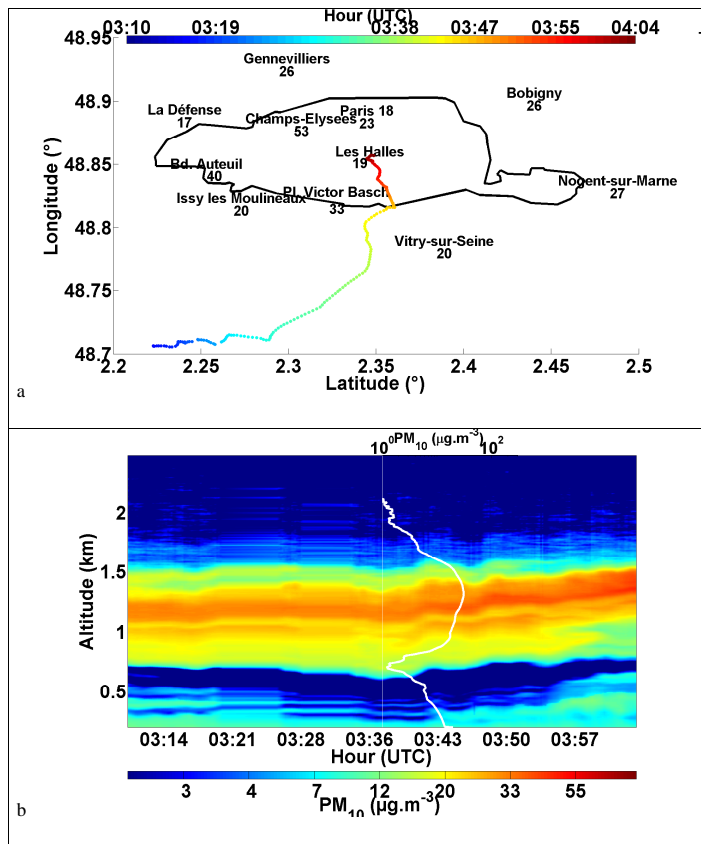


**Fig. 3.** Route followed by the small vehicle embarking the lidar on the 24 May 2005 from Palaiseau to Paris (a), and corresponding 2-D colour-coded temporal evolution of lidar-derived  $PM_{10}$  concentrations (b). Hourly averaged  $PM_{10}$  values measured by AIRPARIF network stations are reported in panel (a). The mean  $PM_{10}$  profile retrieved from lidar signals is shown in white in panel (b).

Title Page

Abstract

Introduction

Conclusions

References

Tables

Figures

◀

▶

◀

▶

Back

Close

Full Screen / Esc

Printer-friendly Version

Interactive Discussion



## Assessment of vertically-resolved $PM_{10}$

J.-C. Raut and  
P. Chazette

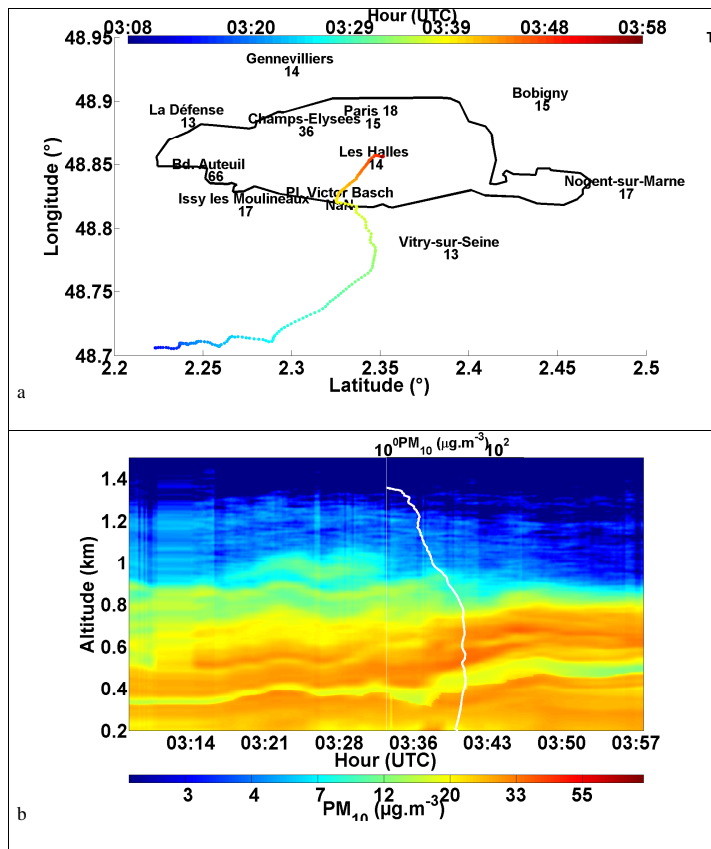
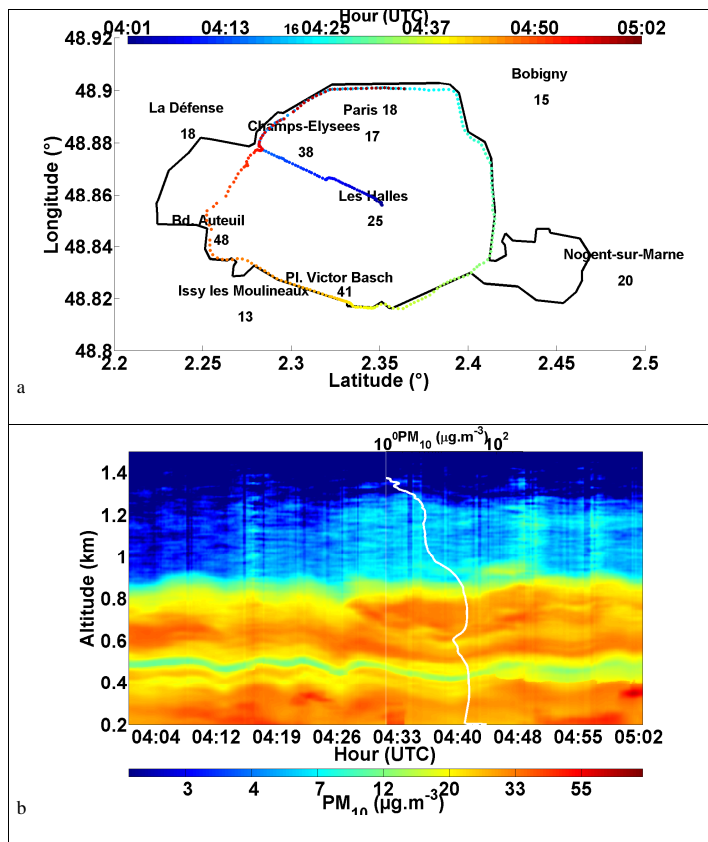


**Fig. 4.** Route followed by the small vehicle embarking the lidar on the 25 May 2005 from Palaiseau to Paris **(a)**, and corresponding 2-D colour-coded temporal evolution of lidar-derived  $PM_{10}$  concentrations **(b)**. Hourly averaged  $PM_{10}$  values measured by AIRPARIF network stations are reported in panel (a). The mean  $PM_{10}$  profile retrieved from lidar signals is shown in white in panel (b).

[Title Page](#)
[Abstract](#)
[Introduction](#)
[Conclusions](#)
[References](#)
[Tables](#)
[Figures](#)
[◀](#)
[▶](#)
[◀](#)
[▶](#)
[Back](#)
[Close](#)
[Full Screen / Esc](#)
[Printer-friendly Version](#)
[Interactive Discussion](#)

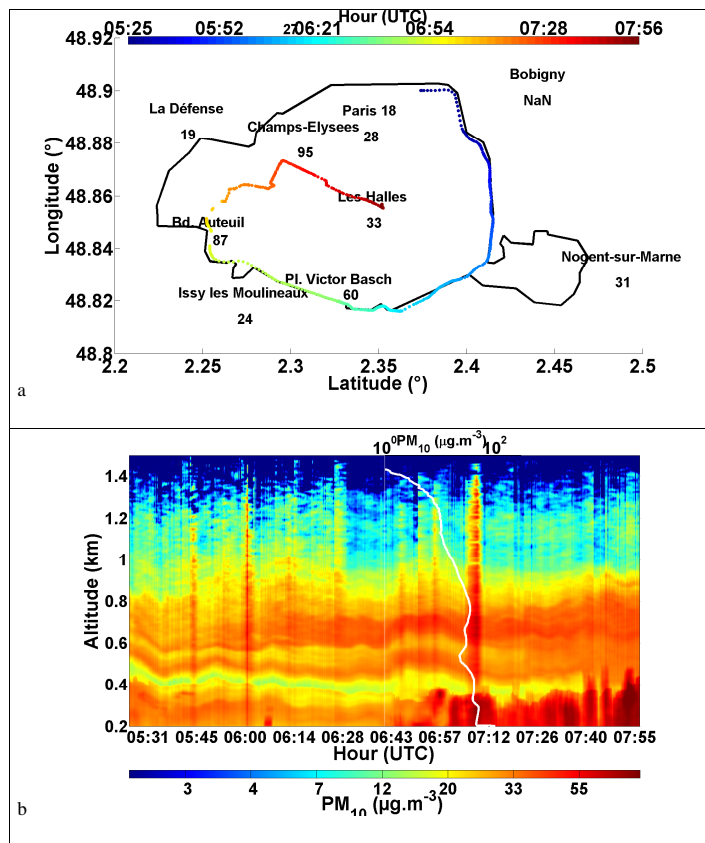
## Assessment of vertically-resolved $PM_{10}$

J.-C. Raut and  
P. Chazette



**Fig. 5.** Route followed by the small vehicle embarking the lidar on the 25 May 2005 the Paris Peripherique before traffic (a), and corresponding 2-D colour-coded temporal evolution of lidar-derived  $PM_{10}$  concentrations (b). Hourly averaged  $PM_{10}$  values measured by AIRPARIF network stations are reported in panel (a). The mean  $PM_{10}$  profile retrieved from lidar signals is shown in white in panel (b).

[Title Page](#)
[Abstract](#)
[Introduction](#)
[Conclusions](#)
[References](#)
[Tables](#)
[Figures](#)
[◀](#)
[▶](#)
[◀](#)
[▶](#)
[Back](#)
[Close](#)
[Full Screen / Esc](#)
[Printer-friendly Version](#)
[Interactive Discussion](#)

Assessment of  
vertically-resolved  
PM<sub>10</sub>J.-C. Raut and  
P. Chazette

**Fig. 6.** Route followed by the small vehicle embarking the lidar on the 25 May 2005 the Paris Peripherique in traffic conditions (a), and corresponding 2-D colour-coded temporal evolution of lidar-derived PM<sub>10</sub> concentrations (b). Hourly averaged PM<sub>10</sub> values measured by AIRPARIF network stations are reported in panel (a). The mean PM<sub>10</sub> profile retrieved from lidar signals is shown in white in panel (b).

[Title Page](#)[Abstract](#)[Introduction](#)[Conclusions](#)[References](#)[Tables](#)[Figures](#)[◀](#)[▶](#)[◀](#)[▶](#)[Back](#)[Close](#)[Full Screen / Esc](#)[Printer-friendly Version](#)[Interactive Discussion](#)

## Assessment of vertically-resolved $PM_{10}$

J.-C. Raut and  
P. Chazette

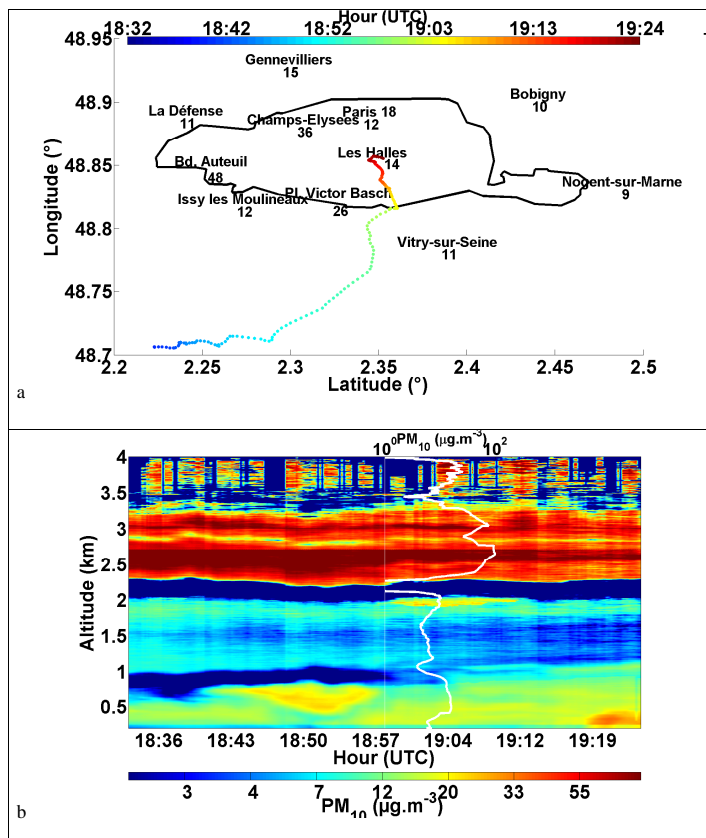


**Fig. 7.** Route followed by the small vehicle embarking the lidar on the 26 May 2005 from Palaiseau to Paris (a), and corresponding 2-D colour-coded temporal evolution of lidar-derived  $PM_{10}$  concentrations (b). Hourly averaged  $PM_{10}$  values measured by AIRPARIF network stations are reported in panel (a). The mean  $PM_{10}$  profile retrieved from lidar signals is shown in white in panel (b).

[Title Page](#)
[Abstract](#)
[Introduction](#)
[Conclusions](#)
[References](#)
[Tables](#)
[Figures](#)
[◀](#)
[▶](#)
[◀](#)
[▶](#)
[Back](#)
[Close](#)
[Full Screen / Esc](#)
[Printer-friendly Version](#)
[Interactive Discussion](#)

## Assessment of vertically-resolved $PM_{10}$

J.-C. Raut and  
P. Chazette

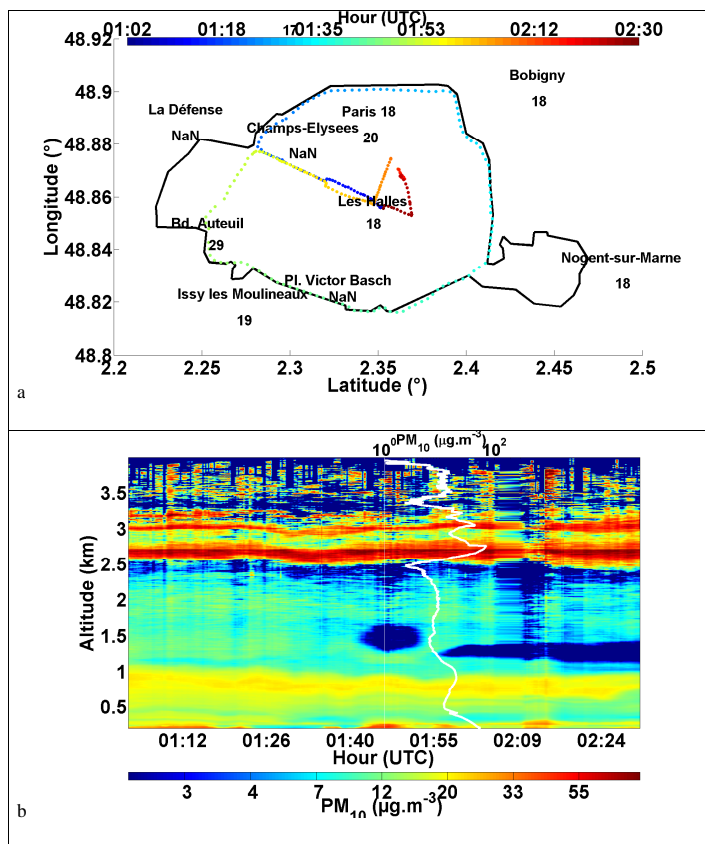
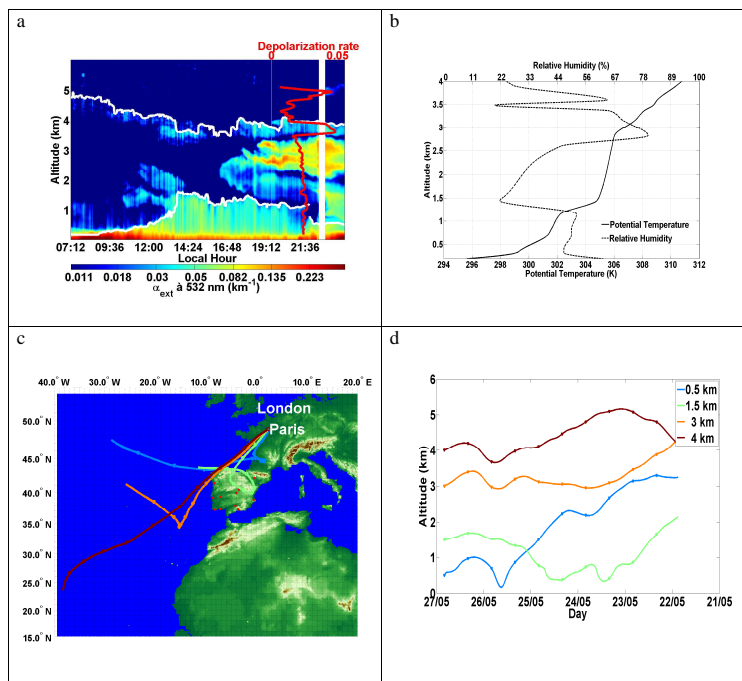


**Fig. 8.** Route followed by the small vehicle embarking the lidar on the 27 May 2005 over the Paris ring (a), and corresponding 2D colour-coded temporal evolution of lidar-derived  $PM_{10}$  concentrations (b). Hourly averaged  $PM_{10}$  values measured by AIRPARIF network stations are reported in panel (a). The mean  $PM_{10}$  profile retrieved from lidar signals is shown in white in panel (b).

[Title Page](#)
[Abstract](#)
[Introduction](#)
[Conclusions](#)
[References](#)
[Tables](#)
[Figures](#)
[◀](#)
[▶](#)
[◀](#)
[▶](#)
[Back](#)
[Close](#)
[Full Screen / Esc](#)
[Printer-friendly Version](#)
[Interactive Discussion](#)

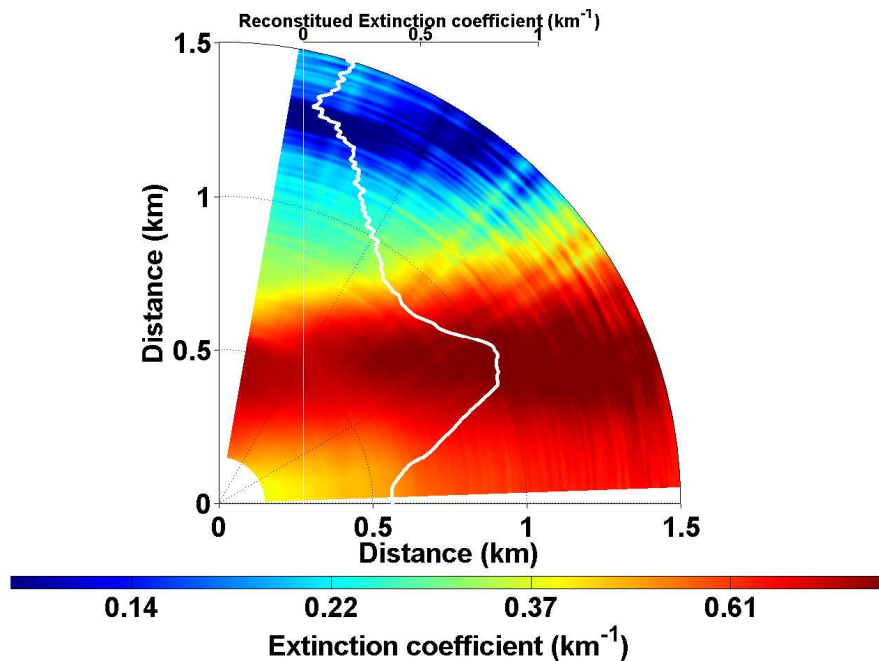
## Assessment of vertically-resolved PM<sub>10</sub>

J.-C. Raut and  
P. Chazette



**Fig. 9.** Temporal evolution of lidar vertical profiles of extinction coefficient at 532 nm measured over Paris city hall on the 26 May 2005 by LESAA lidar **(a)**. The associated vertical profile of the depolarization rate retrieved at 20:00 UTC is shown in red. The mean vertical profiles of RH and potential temperature are represented in **(b)**. Back trajectories for 5-day periods ending over Paris at 20:00 UTC on 26 May at 0.5, 1.5, 3 and 4 km MSL (courtesy of NOAA Air Resources Laboratory <http://www.arl.noaa.gov>) are reported in **(c)**. The triangles give the 12-h spacing. The locations of the fires detected by MODIS products from 21 to 24 May are given by red dots over Spain and Portugal. The location of the air mass for each day against the altitude is given in **(d)**.

[Title Page](#)
[Abstract](#)
[Introduction](#)
[Conclusions](#)
[References](#)
[Tables](#)
[Figures](#)
[◀](#)
[▶](#)
[◀](#)
[▶](#)
[Back](#)
[Close](#)
[Full Screen / Esc](#)
[Printer-friendly Version](#)
[Interactive Discussion](#)

**Assessment of  
vertically-resolved  
PM<sub>10</sub>**J.-C. Raut and  
P. Chazette

**Fig. 10.** Lidar scanning tomography between 0° and 90° performed on the 12 July 2005 over Palaiseau at ~21:00 UTC and represented in aerosol extinction coefficient at 355 nm. The white line gives the reconstituted extinction coefficient from multiangular profiles down to the surface.

[Title Page](#)[Abstract](#)[Introduction](#)[Conclusions](#)[References](#)[Tables](#)[Figures](#)[⏪](#)[⏩](#)[◀](#)[▶](#)[Back](#)[Close](#)[Full Screen / Esc](#)[Printer-friendly Version](#)[Interactive Discussion](#)